

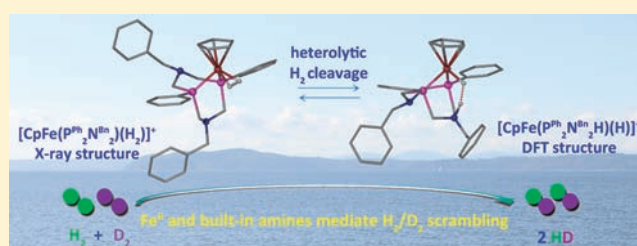
Synthesis, Characterization, and Reactivity of Fe Complexes Containing Cyclic Diazadiphosphine Ligands: The Role of the Pendant Base in Heterolytic Cleavage of H₂

Tianbiao Liu, Shentan Chen, Molly J. O'Hagan, Mary Rakowski DuBois, R. Morris Bullock,* and Daniel L. DuBois*

Chemical and Materials Sciences Division, Pacific Northwest National Laboratory, P.O. Box 999, K2-57, Richland, Washington 99352, United States

S Supporting Information

ABSTRACT: The iron complexes CpFe(P^{Ph}₂N^{Bn}₂)Cl (**1-Cl**), CpFe(P^{Ph}₂N^{Ph}₂)Cl (**2-Cl**), and CpFe(P^{Ph}₂C₅)Cl (**3-Cl**) (where P^{Ph}₂N^{Bn}₂ is 1,5-dibenzyl-1,5-diaza-3,7-diphenyl-3,7-diphosphacyclooctane, P^{Ph}₂N^{Ph}₂ is 1,3,5,7-tetraphenyl-1,5-diaza-3,7-diphosphacyclooctane, and P^{Ph}₂C₅ is 1,4-diphenyl-1,4-diphosphacycloheptane) have been synthesized and characterized by NMR spectroscopy, electrochemical studies, and X-ray diffraction. These chloride derivatives are readily converted to the corresponding hydride complexes [CpFe-(P^{Ph}₂N^{Bn}₂)H (**1-H**), CpFe(P^{Ph}₂N^{Ph}₂)H (**2-H**), CpFe(P^{Ph}₂C₅)H (**3-H**)] and H₂ complexes [CpFe(P^{Ph}₂N^{Bn}₂)(H₂)]BAR^F₄, [1-H₂]⁺BAR^F₄, (where BAR^F₄ is B[(3,5-(CF₃)₂C₆H₃)₄]⁻), [CpFe(P^{Ph}₂N^{Ph}₂)(H₂)]BAR^F₄, [2-H₂]⁺BAR^F₄, and [CpFe(P^{Ph}₂C₅)(H₂)]BAR^F₄, [3-H₂]⁺BAR^F₄, as well as [CpFe(P^{Ph}₂N^{Bn}₂)(CO)]BAR^F₄, [1-CO]Cl. Structural studies are reported for [1-H₂]⁺BAR^F₄, 1-H, 2-H, and [1-CO]Cl. The conformations adopted by the chelate rings of the P^{Ph}₂N^{Bn}₂ ligand in the different complexes are determined by attractive or repulsive interactions between the sixth ligand of these pseudo-octahedral complexes and the pendant N atom of the ring adjacent to the sixth ligand. An example of an attractive interaction is the observation that the distance between the N atom of the pendant amine and the C atom of the coordinated CO ligand for [1-CO]BAR^F₄ is 2.848 Å, considerably shorter than the sum of the van der Waals radii of N and C atoms. Studies of H/D exchange by the complexes [1-H₂]⁺, [2-H₂]⁺, and [3-H₂]⁺ carried out using H₂ and D₂ indicate that the relatively rapid H/D exchange observed for [1-H₂]⁺ and [2-H₂]⁺ compared to [3-H₂]⁺ is consistent with intramolecular heterolytic cleavage of H₂ mediated by the pendant amine. Computational studies indicate a low barrier for heterolytic cleavage of H₂. These mononuclear Fe^{II} dihydrogen complexes containing pendant amines in the ligands mimic crucial features of the distal Fe site of the active site of the [FeFe]-hydrogenase required for H–H bond formation and cleavage.



INTRODUCTION

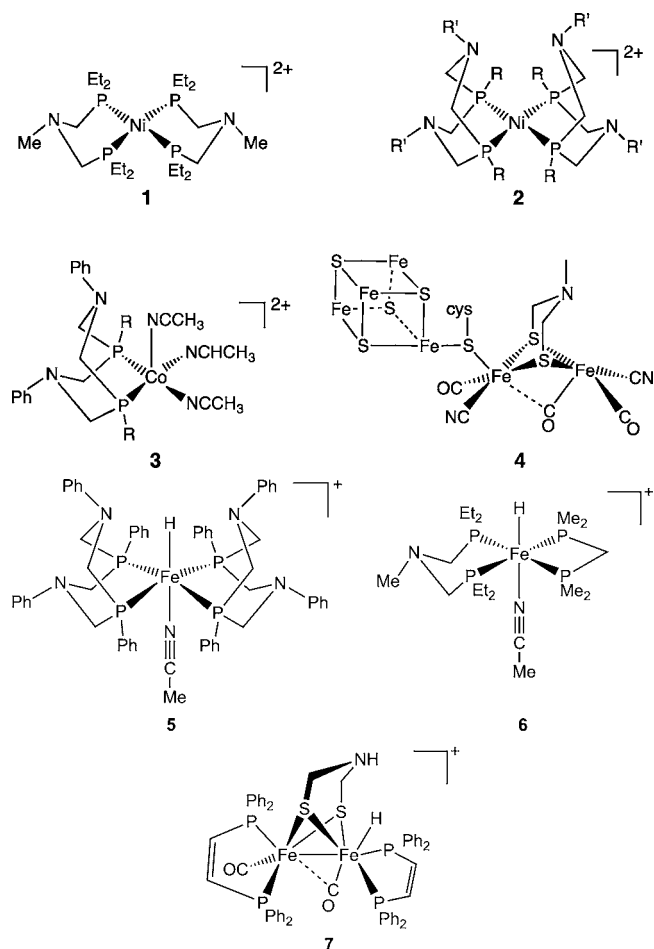
Hydrogenase enzymes are fast and energy-efficient molecular catalysts for hydrogen oxidation and production, and their active sites contain the inexpensive and abundant metals iron and/or nickel.^{1,2} These features have inspired numerous groups to study simpler synthetic molecular electrocatalysts that mimic the structure and/or function of these enzymes that are found in nature.³ Research in our laboratories has focused on transition-metal complexes containing pendant amines incorporated into diphosphine ligands, such as those shown in structures 1–3.^{4–6} These nickel and cobalt complexes are electrocatalysts for either the oxidation or production of hydrogen, and the pendant amines have been shown to play important roles in the catalytic reactions of these complexes by facilitating: (1) heterolytic H–H bond cleavage/formation; (2) the coupling of proton and electron transfer reactions; and (3) proton transfer between acids and bases in solution and the redox active metal center. It is likely that these same functions are also facilitated by the pendant amine of the azadithiolate ligand proposed to be present in the active site of the [FeFe]-hydrogenase enzyme, structure 4.^{2,7}

Because of its high abundance⁸ and low toxicity, iron is a particularly attractive metal for incorporation into synthetic catalysts for the production and oxidation of H₂. Recently studied iron complexes containing an amine base in the second coordination sphere have included simple mononuclear iron complexes, such as 5 and 6,^{9,10} as well as diiron complexes that model the hydrogenase active site, such as 7¹¹ and related derivatives.¹² Studies with several of these compounds have established that the pendant amines can play an important role in relaying protons between metal and solution, in coupling proton and electron transfers and in activating dihydrogen. Nevertheless, the electrocatalytic activity for H₂ formation demonstrated for iron derivatives with pendant amines is often limited by low rates, low stability, and/or high overpotentials. Furthermore, very few examples of Fe complexes are known for H₂ activation, and iron-based molecular electrocatalysts for H₂ oxidation have not been developed.

In this work we describe the syntheses and characterizations of a series of new cyclopentadienyl iron derivatives containing a cyclic

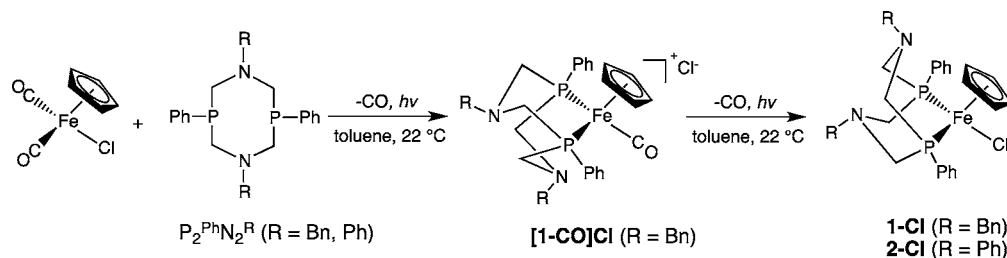
Received: December 8, 2011

Published: March 6, 2012



P^{Ph}₂N^R₂ ligand (1,5-dibenzyl-1,5-diaza-3,7-diphenyl-3,7-diphosphacyclooctane, where R = Bn (benzyl), or 1,3,5,7-tetraphenyl-1,5-diaza-3,7-diphosphacyclooctane, where R = Ph) with the aim of determining how the complexes might be modified and developed to function as electrocatalysts for oxidation or formation of H₂. These complexes have a structural motif that should permit facile tuning of the electronic and steric properties by varying substituents on both the Cp and diphosphine ligand, while incorporating positioned pendant bases to promote facile heterolytic cleavage or formation of the H–H bond. To assess the importance of the amine bases in the second coordination sphere, we have also prepared related CpFe derivatives containing a cyclic diphosphine ligand with no bases in the ligand backbone. The work presented here shows that the potential of the Fe^{III/II} couple and ease of H₂ addition make these complexes interesting potential electrocatalysts for H₂ oxidation. In addition, our studies show that the conformations of the chelate rings of the P^{Ph}₂N^R₂ ligands are determined by attractive or repulsive interactions between the N atom and the sixth ligand of these pseudo-

Scheme 1



octahedral complexes. We also observed that intramolecular heterolytic cleavage of H₂ (as manifested by H/D exchange) is enhanced by a pendant amine. Complete H₂ heterolytic cleavage can be achieved using an external base as proton acceptor. These results indicate a ferrous (Fe^{II}) center and pendant amines in Fe complexes are crucial features for H₂ bonding and cleavage, as proposed for the active site of the [FeFe]-hydrogenase.⁷ Although electrocatalytic oxidation of H₂ is not observed for CpFe-(P^{Ph}₂N^{Bn}₂)H, electrochemical studies indicate that this complex is capable of performing all of the individual steps required for a catalytic process. Thus this work provides a useful basis for catalyst development in this series of CpFe derivatives.

RESULTS

Synthesis and Characterization of CpFe(P^{Ph}₂N^R₂)Cl. A 1:1 mixture of CpFe(CO)₂Cl and P^{Ph}₂N^{Bn}₂ was dissolved in toluene and irradiated with a UV mercury lamp to give CpFe(P^{Ph}₂N^{Bn}₂)Cl (1-Cl), which was isolated in 81% yield (Scheme 1) as black crystals. During the early stages of the photolysis, a yellow solid precipitated that was identified as [CpFe(P^{Ph}₂N^{Bn}₂)(CO)]Cl ([1-CO]Cl). Under prolonged photolysis, this product loses CO to give 1-Cl. Both 1-Cl and [1-CO]Cl were fully characterized by ¹H and ³¹P{¹H} NMR spectroscopy, elemental analyses, and single crystal X-ray diffraction studies. In the ³¹P{¹H} NMR spectrum, CpFe-(P^{Ph}₂N^{Bn}₂)Cl displays a singlet at 57.2 ppm. The ¹H NMR spectrum is also consistent with the formulation of this complex, with resonances assignable to the Cp and P^{Ph}₂N^{Bn}₂ ligands (see Experimental Section and Figure S1, Supporting Information). Similar ¹H and ³¹P{¹H} NMR spectra were observed for [1-CO]Cl. Infrared spectroscopy of [1-CO]Cl in CH₂Cl₂ shows a single carbonyl absorption at 1964 cm⁻¹, consistent with the expected monocarbonyl complex (Figure S2, Supporting Information). A similar photolysis reaction was carried out with a mixture of CpFe(CO)₂Cl and P^{Ph}₂N^{Ph}₂ to form CpFe(P^{Ph}₂N^{Ph}₂)Cl (2-Cl), and spectroscopic data for this product are given in the Experimental Section.

Crystals of 1-Cl and 2-Cl suitable for X-ray diffraction analysis were grown from a CH₂Cl₂ solution layered with hexane. The structures of the two products are very similar, and only data for 1-Cl are discussed here. The structure is depicted in Figure 1a, and selected bond distances and angles are given in Table 1. Figure 1 and Table 1 also provide information about other structures to be presented and discussed later in this paper. The complex 1-Cl adopts a typical three-legged piano-stool geometry. The Fe–Cl and Fe–P bond lengths are similar to those reported for Cp*Fe(dppe)Cl (dppe = 1,2-bis-(diphenylphosphino)ethane).¹³ The bite angle of the P^{Ph}₂N^{Bn}₂ ligand is 81.37(2)°, comparable to the values for this ligand in other Fe,¹⁰ Ni⁵, or Co⁶ complexes. The six-membered ring of the P^{Ph}₂N^{Bn}₂ ligand adjacent to the Cp ligand adopts a boat conformation with the lone pair of the N atom directed toward

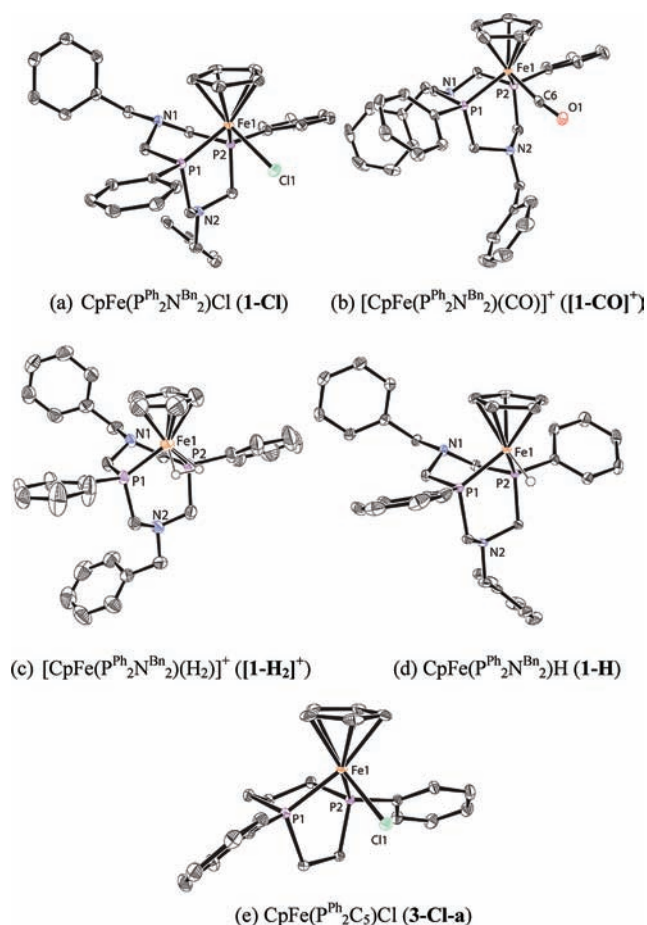


Figure 1. Molecular structures of complexes **1-Cl** (a), $[1\text{-CO}]^+$ (b), $[1\text{-H}_2]^+$ (c), **1-H** (d), and **3-Cl-a** (e) represented as thermal ellipsoid drawings at 50% ellipsoid possibility. The atomic positions of the H_2 ligand of $[1\text{-H}_2]^+$ were not refined but were modeled using appropriate constraints and restraints (see text and Experimental Section for details). Hydrogen atoms are not shown except for the H_2 ligand of $[1\text{-H}_2]^+$ and the Fe-H in **1-H**.

the Cp ring. The second six-membered ring adopts a chair conformation. This orientation presumably avoids repulsion between the lone pair of nitrogen and the chloride ligand.

Crystals of $[1\text{-CO}]\text{Cl}$ were grown from a CH_2Cl_2 solution layered with hexane, and an X-ray diffraction analysis was undertaken. The structure consists of the $[\text{CpFe}(\text{P}^{\text{Ph}}_2\text{N}^{\text{Bn}}_2)(\text{CO})]^+$ cation, chloride anion, and one equivalent of diethyl ether. A drawing of $[\text{CpFe}(\text{P}^{\text{Ph}}_2\text{N}^{\text{Bn}}_2)(\text{CO})]^+$ is shown in Figure 1b,

and bond distances and angles are listed in Table 1. The overall structure is similar to **1-Cl**, with slightly longer Fe–P bond distances. A particularly interesting feature of this complex is that in the $\text{P}^{\text{Ph}}_2\text{N}^{\text{Bn}}_2$ ligand, the chelate ring proximal to the Cp ligand has a chair conformation, while a boat conformation is observed for the ring adjacent to the CO ligand. This is the only complex of this class that we have studied that has this stereochemistry in the solid state. A clue to the origin of the boat conformation is found in the $\text{N}\cdots\text{CO}$ distance of 2.848 Å. This distance is shorter than the sum of van der Waals radii of N and C atoms (3.25 Å)¹⁴ by ca. 0.4 Å, indicating there is a significant bonding interaction between the N atom of the $\text{P}^{\text{Ph}}_2\text{N}^{\text{Bn}}_2$ ligand and the C atom of the carbonyl ligand. As a result, the Fe–C–O angle, 170.97(17)°, is not linear.

Synthesis and Characterization of $[\text{CpFe}(\text{P}^{\text{Ph}}_2\text{N}^{\text{R}}_2)(\text{H}_2)]\text{-BAR}^{\text{F}}_4$ and $[\text{CpFe}(\text{P}^{\text{Ph}}_2\text{N}^{\text{R}}_2)(\text{HD})]\text{BAR}^{\text{F}}_4$. The dihydrogen complex, $[\text{CpFe}(\text{P}^{\text{Ph}}_2\text{N}^{\text{Bn}}_2)(\text{H}_2)]\text{BAR}^{\text{F}}_4$, $[1\text{-H}_2]\text{BAR}^{\text{F}}_4$, (Ar^{F} = 3,5-bis(trifluoromethyl)phenyl) was synthesized from **1-Cl** by abstracting chloride using $\text{NaBAR}^{\text{F}}_4$ in fluorobenzene (PhF) under an atmosphere of H_2 (1.0 atm). This synthesis can also be carried out in a two-step process by abstracting chloride first to form a brown solution of a cationic complex $[\text{CpFe}(\text{P}^{\text{Ph}}_2\text{N}^{\text{Bn}}_2)]\text{BAR}^{\text{F}}_4$ designated as $[1]^+$, then adding H_2 gas to form a yellow solution of $[1\text{-H}_2]\text{BAR}^{\text{F}}_4$, as shown in Scheme 2. When CH_3CN was used as solvent for the above

Scheme 2

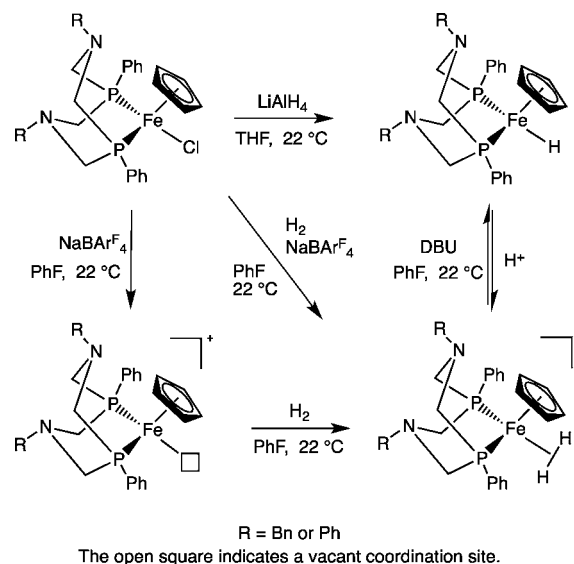


Table 1. Selected Bond Distances (Å) and Angles (°) for Complexes **1-Cl**, $[1\text{-CO}]^+$, $[1\text{-H}_2]^+$, **1-H**, and **3-Cl-a**

	1-Cl	$[1\text{-CO}]^+$	$[1\text{-H}_2]^+$	1-H	3-Cl-a
Fe–Cp (centroid)	1.7047(9)	1.7234(10)	1.6986(21)	1.6886(8)	1.6930(6)
Fe–X ^a	2.3180(7)	1.759(2)	1.60(2)	1.47(2)	2.3164(3)
Fe–P1	2.1523(7)	2.1989(6)	2.1830(14)	2.1008(5)	2.1810(3)
Fe–P2	2.1568(7)	2.1772(6)	2.1799(15)	2.1014(5)	2.1672(3)
Cp–Fe–P1	125.81	123.99	124.98	128.37	129.09
Cp–Fe–P2	127.10	126.13	128.43	130.77	128.00
Cp–Fe–X	123.03	123.08	121.28	125.73	124.23
P1–Fe–P2	81.37(2)	81.66(2)	81.04(5)	82.069(19)	78.426(12)
P1–Fe–X	94.74(2)	97.94(7)	84.0(8)	87.5(8)	91.542(13)
P2–Fe–X	93.41(2)	93.46(6)	83.8(8)	87.5(8)	91.942(13)

^aX represents the atom of the monodentate ligand coordinated to Fe. For $[1\text{-H}_2]^+$, the distance of Fe–(H_2) is 1.535 Å (center of the H–H bond) and the angle of Cp–Fe–(H_2) is 121.82°.

reactions, $[\mathbf{1-H}_2]\text{BAR}_4^{\text{F}}$ was not formed because of coordination of CH_3CN to the iron. Complex $[\mathbf{1-H}_2]^+$ shows a singlet in the ^{31}P NMR spectrum at 58.4 ppm, and the ^1H NMR spectrum exhibits a broad singlet at -12.64 ppm assigned to the H_2 ligand (see Figure 2a). Further support for the assignment of

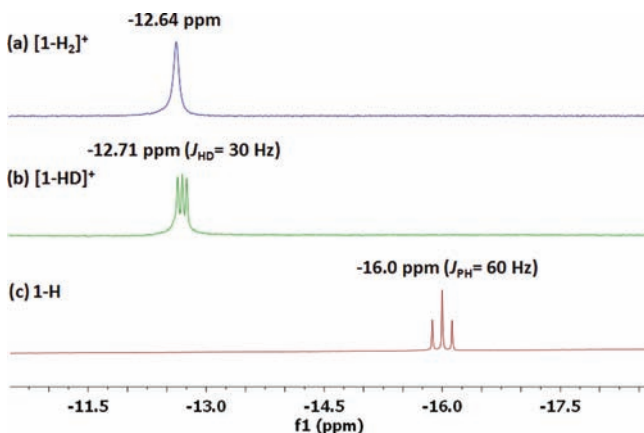


Figure 2. (a) ^1H NMR spectrum (PhCl-d_3) of $[\text{CpFe}(\text{P}^{\text{Ph}}_2\text{N}^{\text{Bn}}_2)(\text{H}_2)]\text{BAR}_4^{\text{F}}$, $[\mathbf{1-H}_2]\text{BAR}_4^{\text{F}}$, showing the H_2 resonance, (b) ^1H NMR spectrum (PhCl-d_3) of $[\text{CpFe}(\text{P}^{\text{Ph}}_2\text{N}^{\text{Bn}}_2)(\text{HD})]\text{BAR}_4^{\text{F}}$, $[\mathbf{1-HD}]\text{BAR}_4^{\text{F}}$, showing the HD resonance, and (c) ^1H NMR spectrum (THF-d_8) of $[\text{CpFe}(\text{P}^{\text{Ph}}_2\text{N}^{\text{Bn}}_2)(\text{H})]$, $\mathbf{1-H}$, showing the hydride resonance. All spectra were recorded at 22°C .

$[\mathbf{1-H}_2]^+$ as a metal dihydrogen complex was obtained by preparation of the corresponding $[\text{Fe}(\text{HD})]^+$ complex, $[\mathbf{1-HD}]^+$, which exhibits a 1:1:1 triplet at -12.71 ppm ($J_{\text{HD}} = 30$ Hz, see Figure 2b) for the HD ligand. This HD resonance shows an isotopic shift (-0.07 ppm) compared to the H_2 ligand of $[\mathbf{1-H}_2]^+$.¹⁵ The HD coupling constant is comparable to those of $[\text{CpFe}(\text{dppp})(\text{HD})]\text{BF}_4$ (30.7 Hz) and $[\text{CpFe}(\text{dppe})(\text{HD})]\text{BF}_4$ (29.0 Hz).¹⁶ Based on the J_{HD} , the H–H distance of the dihydrogen ligand of $[\mathbf{1-H}_2]^+$ is calculated to be 0.94 Å using the equation of Heinekey¹⁷ or 0.92 Å using the equation of Morris.^{18,19} Due to the low solubility of $[\mathbf{1-H}_2]\text{BAR}_4^{\text{F}}$ below -20°C , the T_1 of the dihydrogen ligand was measured at 22°C and was found to be 14 ms, consistent with a dihydrogen complex.

Crystals of $[\mathbf{1-H}_2]\text{BAR}_4^{\text{F}}$ were grown from a fluorobenzene solution layered with hexane under H_2 (1.0 atm). The structure of the cation $[\mathbf{1-H}_2]^+$, as determined by an X-ray diffraction study, is shown in Figure 1c. The overall structure, the Fe–P bond distances, and the P1–Fe–P2 angle of the cation are quite similar to its precursor ($\mathbf{1-Cl}$). Since the H_2 ligand cannot be accurately located using X-ray diffraction data, the single residue ca. 1.60 Å from the Fe atom was modeled and refined as an H_2 ligand. The H–H bond distance was constrained using the distance (0.94 Å) derived from the NMR study of $[\mathbf{1-HD}]^+$.

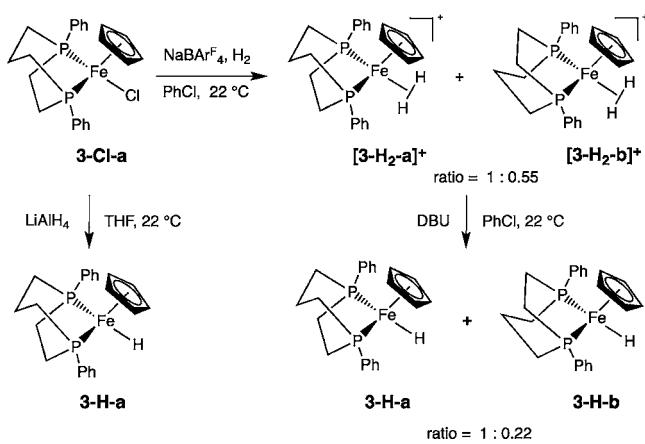
Synthesis and Characterization of $\text{CpFe}(\text{P}^{\text{Ph}}_2\text{N}^{\text{R}}_2)(\text{H})$. $[\mathbf{1-H}_2]^+$ can be readily deprotonated by DBU (1,8-diazabicyclo[5.4.0]undec-7-ene, $\text{p}K_a = 24$ for H-DBU^+ in CH_3CN)²⁰ in PhF solvent to generate the orange hydride complex, $[\text{CpFe}(\text{P}^{\text{Ph}}_2\text{N}^{\text{Bn}}_2)(\text{H})]$ ($\mathbf{1-H}$), which was isolated in 20% yield. Reversible protonation of $\mathbf{1-H}$ with 1 equiv of $\text{HBF}_4\cdot\text{Et}_2\text{O}$ leads to the clean formation of the $[\text{Fe-H}_2]^+$ complex $[\mathbf{1-H}_2]^+$, as indicated by NMR spectroscopy. Attempts to deprotonate $[\mathbf{1-H}_2]^+$ with excess Et_3N (20 equiv; $\text{p}K_a = 18.8$ in CH_3CN)²⁰ did not result in the formation of the hydride, $\mathbf{1-H}$; no change

was observed in the dihydrogen resonance at -12.64 ppm. These results suggest that the $\text{p}K_a$ of $[\mathbf{1-H}_2]^+$ can be bracketed between 20 and 24. Although these reactions were carried out in fluorobenzene, the $\text{p}K_a$ values cited are for acetonitrile as the solvent. $\mathbf{1-H}$ can also be prepared from $\mathbf{1-Cl}$ by reaction with LiAlH_4 in THF (61% isolated yield). Other metal hydrides, including NaBH_4 , NaH , PPNBH_4 , and LiBEt_3H , were examined for the same reaction but gave lower yields. $\mathbf{1-H}$ shows a singlet at 71.8 ppm in the ^{31}P NMR spectrum and a triplet at -16.0 ppm ($J_{\text{PH}} = 60$ Hz, see Figure 2c) for the hydride in the ^1H NMR spectrum. Crystals of $\mathbf{1-H}$ were grown from an ether solution cooled to -35°C . The crystal structure of $\mathbf{1-H}$ (Figure 1d) is very similar to that of $\mathbf{1-Cl}$, with Fe–P distances and a P1–Fe–P2 angle comparable to those of the other derivatives with the $\text{P}^{\text{Ph}}_2\text{N}^{\text{Bn}}_2$ ligand. The Fe–H distance is $1.47(2)$ Å, a value comparable to that of $[\text{CpFe}(\text{PPh}_3)_2\text{H}]$ (1.49 Å) and shorter than $[\text{CpFe}(\text{dppm})\text{H}]$ (1.59 Å).²¹ It is noted that the P–Fe–X angle (87.5° , $X = \text{H}$ for $\mathbf{1-H}$) is smaller than the values observed for $\mathbf{1-Cl}$ and $[\mathbf{1-CO}]^+$, by as much as 6° , indicating a reduced repulsion between the $\text{P}^{\text{Ph}}_2\text{N}^{\text{Bn}}_2$ ligand and the smaller hydride ligand, though all of these comparisons of Fe–H distances are subject to uncertainty of determination of H locations by X-ray crystallography.²²

Iron derivatives containing the $\text{P}^{\text{Ph}}_2\text{N}^{\text{Ph}}_2$ ligand ($[\mathbf{2-H}_2]^+$, $[\mathbf{2-HD}]^+$, and $\mathbf{2-H}$) were prepared from $\mathbf{2-Cl}$ following procedures similar to those described above. $[\text{CpFe}(\text{P}^{\text{Ph}}_2\text{N}^{\text{Ph}}_2)(\text{H}_2)]\text{BAR}_4^{\text{F}}$ ($[\mathbf{2-H}_2]\text{BAR}_4^{\text{F}}$) shows a singlet at 50.6 ppm in the ^{31}P NMR spectrum and a broad singlet at -12.68 ppm for the dihydrogen ligand in the ^1H NMR spectrum (Figure S6a, Supporting Information). The corresponding $[\text{Fe-HD}]$ species, $[\text{CpFe}(\text{P}^{\text{Ph}}_2\text{N}^{\text{Ph}}_2)(\text{HD})]\text{BAR}_4^{\text{F}}$ ($[\mathbf{2-HD}]\text{BAR}_4^{\text{F}}$), exhibits a 1:1:1 triplet at -12.75 ppm ($J_{\text{HD}} = 27.5$ Hz, see Figure S6b, Supporting Information), indicating a H–H distance of 0.98 Å¹⁷ (or 0.96 Å)^{18,19} for the coordinated H_2 ligand, ca. 0.042 Å longer than the H_2 ligand of $[\mathbf{1-H}_2]^+$. $[\text{CpFe}(\text{P}^{\text{Ph}}_2\text{N}^{\text{Ph}}_2)(\text{H})]$ ($\mathbf{2-H}$) displays a singlet at 73.3 ppm in the ^{31}P NMR spectrum and a triplet hydride signal at -15.74 ppm ($J_{\text{PH}} = 50$ Hz, see Figure S6c, Supporting Information) in the ^1H NMR spectrum. X-ray diffraction studies of $\mathbf{2-Cl}$ and $\mathbf{2-H}$ indicate that the structural parameters of these complexes are similar to those of the corresponding $\text{P}^{\text{Ph}}_2\text{N}^{\text{Bn}}_2$ derivative (Figure S29, Supporting Information).

Synthesis and Characterization of $\text{CpFe}(\text{P}^{\text{Ph}}_2\text{C}_5)\text{Cl}$ ($\mathbf{3-Cl}$), $[\text{CpFe}(\text{P}^{\text{Ph}}_2\text{C}_5)(\text{H}_2)]\text{BAR}_4^{\text{F}}$ ($[\mathbf{3-H}_2]\text{BAR}_4^{\text{F}}$), and $\text{CpFe}(\text{P}^{\text{Ph}}_2\text{C}_5)\text{H}$ ($\mathbf{3-H}$). Attempts were made to prepare $\text{CpFe}(\text{P}^{\text{Ph}}_2\text{C}_6)\text{Cl}$, where $\text{P}^{\text{Ph}}_2\text{C}_6$ ²³ (1,5-diphenyl-1,5-diphosphacyclooctane) is an eight-membered cyclic diphosphine ligand with methylene groups substituted for the amine bases of $\text{P}^{\text{Ph}}_2\text{N}^{\text{R}}_2$ ligands. These complexes would provide structurally analogous control complexes for evaluating the effects of the pendant amines of $[\mathbf{1-H}_2]\text{BAR}_4^{\text{F}}$, $\mathbf{1-H}$, $[\mathbf{2-H}_2]\text{BAR}_4^{\text{F}}$, and $\mathbf{2-H}$ on their structures and reactivities. Unfortunately, the reaction of $[\text{CpFe}(\text{CO})_2\text{Cl}]$ with $\text{P}^{\text{Ph}}_2\text{C}_6$ ²³ did not form the desired mononuclear product $\text{CpFe}(\text{P}^{\text{Ph}}_2\text{C}_6)\text{Cl}$. However, reactions with the closely related seven-membered cyclic diphosphine, $\text{P}^{\text{Ph}}_2\text{C}_5$ ²⁴ (1,4-diphenyl-1,4-diphosphacycloheptane), were successful. The complexes $\text{CpFe}(\text{P}^{\text{Ph}}_2\text{C}_5)\text{Cl}$ ($\mathbf{3-Cl}$), $[\text{CpFe}(\text{P}^{\text{Ph}}_2\text{C}_5)(\text{H}_2)]\text{BAR}_4^{\text{F}}$ ($[\mathbf{3-H}_2]\text{BAR}_4^{\text{F}}$), and $\text{CpFe}(\text{P}^{\text{Ph}}_2\text{C}_5)\text{H}$ ($\mathbf{3-H}$) were prepared using synthetic routes analogous to those used to prepare $\mathbf{1-Cl}$, $[\mathbf{1-H}_2]\text{BAR}_4^{\text{F}}$, and $\mathbf{1-H}$. From the reaction of $[\text{CpFe}(\text{CO})_2\text{Cl}]$ with $\text{P}^{\text{Ph}}_2\text{C}_5$, two isomeric products, $\mathbf{3-Cl-a}$ and $\mathbf{3-Cl-b}$, were observed by $^{31}\text{P}\{^1\text{H}\}$ NMR spectroscopy, with resonances at 80.1 and 85.5 ppm in a ratio of ca. 1.00:0.15.

Scheme 3

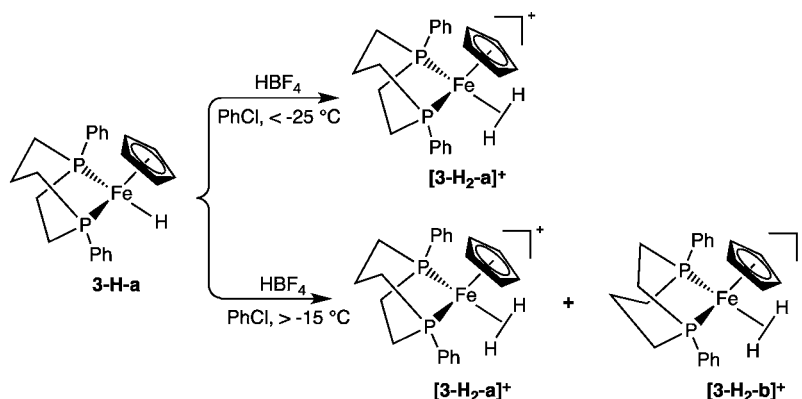


The major isomer (3-Cl-a, Scheme 3) was isolated as a crystalline material. The ^1H NMR spectrum of 3-Cl-a (see Figure S4, Supporting Information) displays a singlet at 4.08 ppm for the Cp ligand and multiplets from 2.66 to 1.80 ppm for the methylene groups of the $\text{P}^{\text{Ph}}_2\text{C}_5$ ligand (see Experimental Section). To provide further information on the structure of this isomer, a single crystal X-ray diffraction study was undertaken (Figure 1e, Table 1). This isomer has a six-membered ring in the chair conformation adjacent to the Cp ring, and the five-membered ring is adjacent to the chloride ligand. The minor isomer, 3-Cl-b, is therefore assigned a structure in which the five-membered chelate ring of the diphosphine is adjacent to the Cp ligand and the six-membered ring is adjacent to the chloride ligand. From Table 1 it can be seen that the Fe–Cl and Fe–P bond distances of 3-Cl-a are comparable to those of 1-Cl and 2-Cl, but the P–Fe–P bite angle is $78.426(12)^\circ$, about $3\text{--}4^\circ$

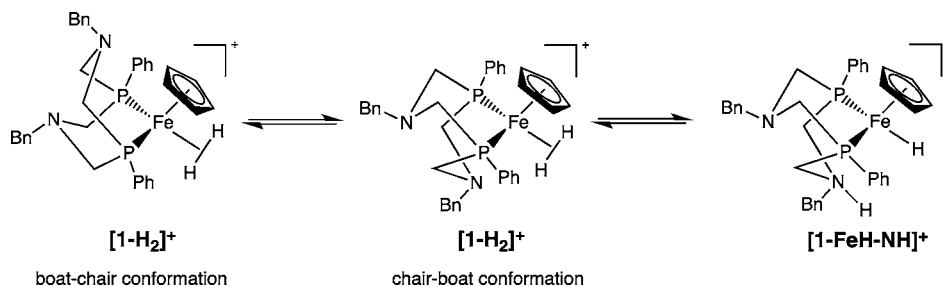
smaller than those of 1-Cl and 2-Cl. This is a consequence of replacing one six-membered chelate ring with a smaller five-membered ring. The change in ring size also reduces the steric interactions between the diphosphine ligand and the chloride and Cp ligands; as a result the P–Fe–Cl and Cp–Fe–P angles (measured to the centroid of the Cp ring) are larger for 3-Cl-a than those of 1-Cl and 2-Cl.

When the pure isomer 3-Cl-a was used as the starting material in the reaction with NaBARF_4 and H_2 , two isomers of $[\text{CpFe}(\text{P}^{\text{Ph}}_2\text{C}_5)(\text{H}_2)]^+$, $[\text{3-H}_2\text{-a}]^+$ and $[\text{3-H}_2\text{-b}]^+$ (ca. 1.00: 0.55, see Scheme 3), were observed by ^1H NMR and $^{31}\text{P}\{^1\text{H}\}$ NMR spectroscopy. The major ($[\text{3-H}_2\text{-a}]^+$) and minor ($[\text{3-H}_2\text{-b}]^+$) isomers exhibit dihydrogen resonances at -13.79 and -13.04 ppm, respectively, in the ^1H NMR spectrum (see Figure S7a, Supporting Information). T_1 values measured at 22°C for the dihydrogen ligand are 22.9 and 19.1 ms for $[\text{3-H}_2\text{-a}]^+$ and $[\text{3-H}_2\text{-b}]^+$, respectively, and the two isomers of the HD complex $[\text{CpFe}(\text{P}^{\text{Ph}}_2\text{C}_5)(\text{HD})]^+$ exhibit two triplets of triplets at -13.89 ppm ($J_{\text{HD}} = 25$, $J_{\text{PH}} = 8.3$ Hz) and -13.13 ppm ($J_{\text{HD}} = 25$, $J_{\text{PH}} = 4.5$ Hz) in the ^1H NMR spectrum (see Figure S7b, Supporting Information), confirming the presence of an H_2 ligand. The J_{HD} value can be used to calculate a H–H distance of 1.02 \AA (or 1.00 \AA) for both isomers.^{17–19} The smaller coupling constant is assigned to the coupling of the proton of H–D to the two phosphorus atoms, and was confirmed by a $^1\text{H}\{^{31}\text{P}\}$ NMR spectrum (see Figure S7c, Supporting Information). Although P–H coupling in dihydrogen complexes is generally not observed, it has been found in some cases. Similar P–H coupling constants have been reported previously for $\text{W}(\text{HD})(\text{CO})_3(\text{P}(i\text{-Pr})_3)_2$ (2.7 Hz)²⁵ and $[\text{CpRu}(\text{P}_2)(\text{HD})]\text{BF}_4$ (3.5 Hz for $\text{P}_2 = 1,2\text{-bis}(\text{dimethylphosphino})\text{ethane}$; 2.3 Hz for $\text{P}_2 = 1,1\text{-dimethyl-2,2-diphenylphosphino}(\text{ethane})$).¹⁵ Resonances corresponding to these two dihydrogen species were observed in the $^{31}\text{P}\{^1\text{H}\}$ NMR spectrum at 83.70 and 85.47 ppm.

Scheme 4



Scheme 5



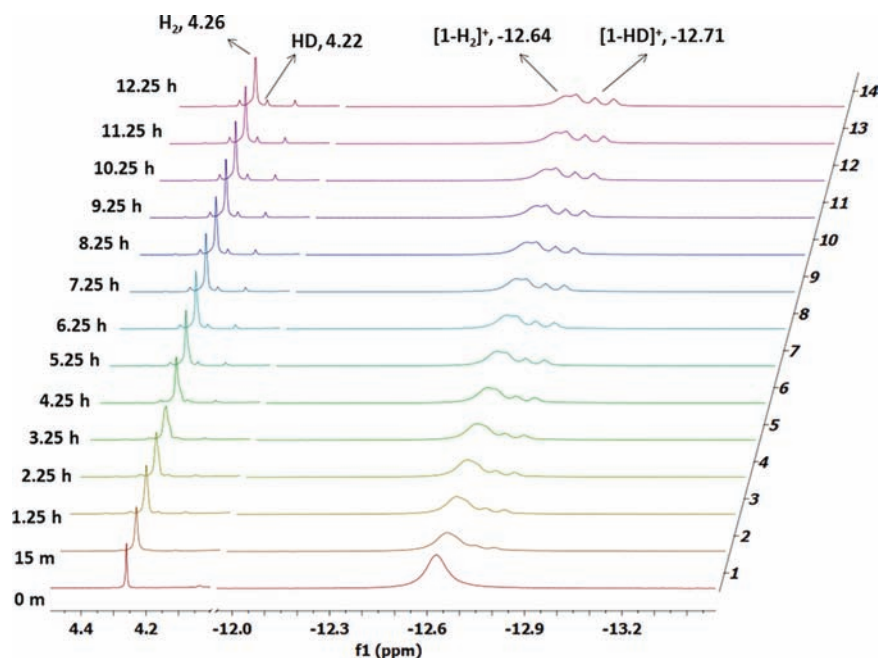
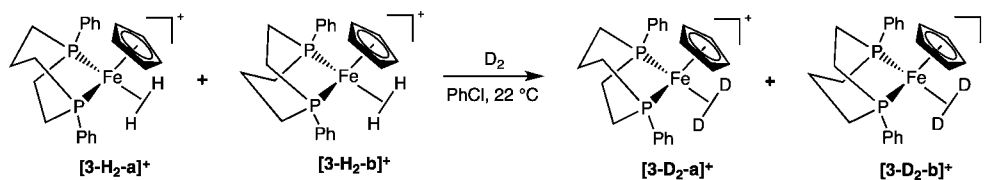


Figure 3. ^1H NMR spectra at 22 °C of $[\text{1-H}_2]^+$ in chlorobenzene- d_5 under D_2 and H_2 as a function of time.

Scheme 6



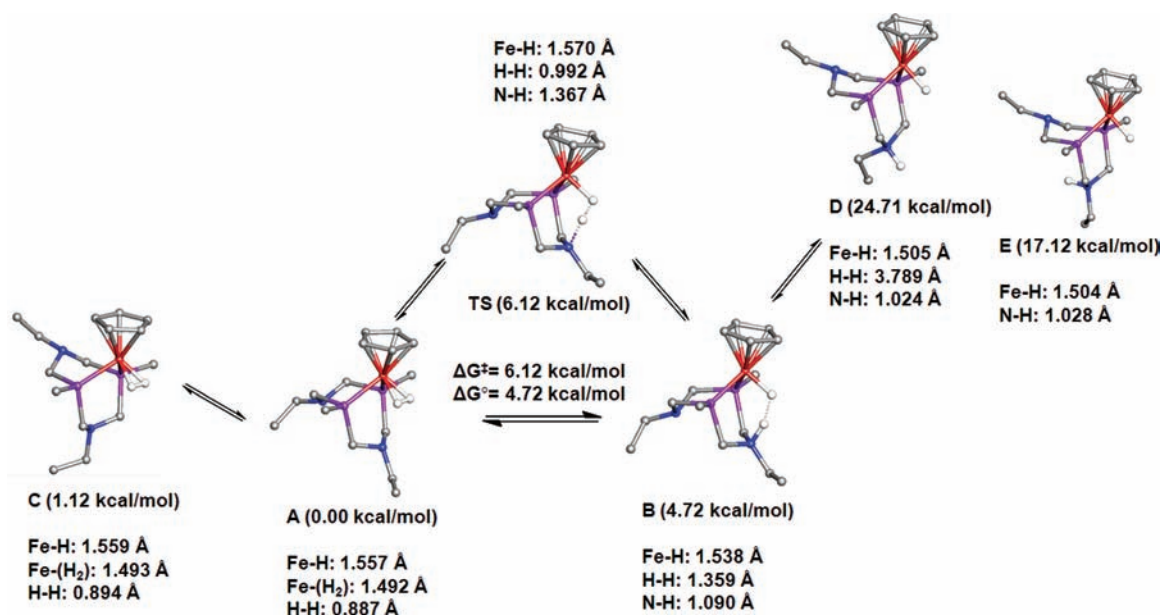
Deprotonation of a mixture of $[\text{3-H}_2\text{-a}]^+$ and $[\text{3-H}_2\text{-b}]^+$ with DBU resulted in two $[\text{Fe-H}]$ isomers, 3-H-a and 3-H-b (see Scheme 3). These isomers exhibit singlets at 96.1 and 100.0 ppm in a ratio of 1.00:0.22 in the $^{31}\text{P}\{^1\text{H}\}$ NMR spectrum. Corresponding hydride resonances are observed as triplets at -17.30 ($J_{\text{PH}} = 65$ Hz) and -15.80 ppm ($J_{\text{PH}} = 65$ Hz) in the ^1H NMR spectrum (see Figure S8a, Supporting Information). The isomer with a phosphorus resonance at 96.1 ppm can be selectively prepared from 3-Cl-a (see Figure S8b, Supporting Information) by reaction with LiAlH_4 . As a result, this isomer is tentatively assigned structure 3-H-a , and the minor isomer is assigned structure 3-H-b (Scheme 4). In order to assign the structures of the two isomers of $[\text{3-H}_2]^+$, protonation of $[\text{CpFe}(\text{P}^{\text{Ph}}_2\text{C}_5)\text{H}]$ (3-H-a) with $\text{HBF}_4\cdot\text{Et}_2\text{O}$ was examined by ^1H NMR spectroscopy at -35 °C. At this temperature only, the major isomer at -13.79 ppm was observed (see Figure S9, Supporting Information), which suggests structure $[\text{3-H}_2\text{-a}]^+$ (see Scheme 4). Upon warming to -15 °C, the resonance for the minor isomer assigned to $[\text{3-H}_2\text{-b}]^+$ appeared at -13.04 ppm. It is proposed that the conversion of $[\text{3-H}_2\text{-a}]^+$ to $[\text{3-H}_2\text{-b}]^+$ proceeds through dissociation of H_2 from $[\text{3-H}_2\text{-a}]^+$ to form the coordinately unsaturated $[\text{CpFe}(\text{P}^{\text{Ph}}_2\text{C}_5)]^+$ species and reassociation of H_2 to form $[\text{3-H}_2\text{-b}]^+$. The lability of the H_2 ligand is indicated by the H_2/D_2 ligand exchange observed for $[\text{3-H}_2]^+$ (vide infra and see Figures S13 and S14, Supporting Information).

H_2/D_2 and H/D Exchange for $[\text{1-H}_2]\text{BAR}^{\text{F}}_4$, $[\text{2-H}_2]\text{BAR}^{\text{F}}_4$, and $[\text{3-H}_2]\text{BAR}^{\text{F}}_4$. To assess the existence of an equilibrium between $[\text{1-H}_2]^+$ and its tautomer, $[\text{1-FeH-NH}]^+$, in which heterolytic cleavage of H_2 has occurred (Scheme 5), H_2/D_2

scrambling experiments were carried out with $[\text{1-H}_2]^+$. In these experiments, a solution was prepared in situ under 1.0 atm of H_2 in an NMR tube, and D_2 (3.0 mL at 1.0 atm) was injected into the NMR tube. Scrambling of H/D was monitored by ^1H NMR spectroscopy (see Figure 3). The formation of $[\text{1-HD}]^+$ was observed after 15 min as a small shoulder at -12.71 ppm on the H_2 resonance of $[\text{1-H}_2]^+$. After 6 h, $[\text{1-HD}]^+$ was the dominant species, as indicated by its distinctive triplet in the ^1H NMR spectrum. During the course of H/D scrambling, the total amount of $[\text{1-H}_2]^+$ and $[\text{1-HD}]^+$ decreased due to formation of $[\text{1-D}_2]^+$, which was confirmed by ^2H NMR (see Figure S10, Supporting Information). After 12 h, the ratio of $[\text{1-H}_2]^+$, $[\text{1-HD}]^+$, and $[\text{1-D}_2]^+$ was 38:51:11. HD gas in solution was also detected ^1H NMR spectroscopy as a triplet at 4.22 ppm ($J_{\text{HD}} = 45$ Hz) (see Figure 3). Based on the integration of the Cp and HD resonances, the concentration of HD gas in solution was determined to be 2.1 mM after 12 h. $[\text{2-H}_2]^+$ was also examined for H/D exchange under the same conditions. The formation of $[\text{2-HD}]^+$ and HD was established by ^1H and ^2H NMR spectroscopy (see Figures S11 and S12, Supporting Information), and after 12 h the ratio of $[\text{2-H}_2]^+$, $[\text{2-HD}]^+$, and $[\text{2-D}_2]^+$ was 28: 51: 20. The concentration of HD gas in the reaction solution was determined by ^1H NMR spectroscopy to be 2.7 mM after 12 h, which suggests $[\text{2-H}_2]^+$ undergoes H/D exchange at a rate comparable to that of $[\text{1-H}_2]^+$.

Complex $[\text{3-H}_2]^+$ was also studied for H_2/D_2 and H/D exchange under identical conditions to those used for $[\text{1-H}_2]^+$ and $[\text{2-H}_2]^+$. Integration of the H_2 resonances for both isomers of $[\text{3-H}_2]^+$ relative to the Cp resonance indicated a decrease in

Scheme 7. DFT Studies of Intramolecular Heterolytic H₂ Cleavage of [1-H₂]⁺: Energy Comparison of Isomers of [1-H₂]⁺ and the Product of Heterolytic Cleavage, [1-FeH-NH]⁺, and Selected Distances^a



^aFor clarity, phenyl substituents of all structures are simplified by only showing ipso carbons.

the intensity of the H₂ resonance with time, and a ²H NMR spectrum recorded after 4 h confirmed the presence of two [Fe(D₂)⁺ isomers (see Scheme 6 and Figures S13 and S14, Supporting Information). The formation of [3-D₂]⁺ via H₂/D₂ exchange was also observed by ³¹P{¹H} NMR spectroscopy. However, after 19 h there was no detectable formation of an [Fe(HD)]⁺ species or HD gas that would indicate cleavage of the H–H or D–D bonds or H/D exchange. Addition of 2.0 equiv of either aniline or benzylamine resulted in the slow formation of [3-HD]⁺ and HD gas over 12 h.

In experiments using aniline as an external base (Figures S15 and S16, Supporting Information), the concentration of HD gas in the reaction solution after 12 h was determined to be 0.96 mM, less than half of that observed for [1-H₂]⁺ and 2-H₂⁺, indicating that the pendant bases in the latter complexes are important for catalyzing H/D exchange more efficiently than [3-H₂]⁺ in the presence of an external base and much more efficiently than [3-H₂]⁺ alone.

Deuterium Incorporation from D₂O into [CpFe(P^{Ph}₂N^R₂)(H)] (R = Ph, Bn) and [CpFe(P^{Ph}₂C₅)(H)]. In the presence of excess D₂O (56 equiv, 0.93 M) in THF, all three hydrides (0.017 M, 1-H, 2-H, and 3-H-a) undergo exchange of the hydride ligand for deuterium to form the corresponding [Fe-D] species within 4 min. The half-life for the reaction can be estimated as 2 min, but differences in the rates of exchange are not distinguishable for the three hydride complexes using this approach.

Computational Studies of the Heterolytic Cleavage of Dihydrogen by [CpFe(P^{Ph}₂N^{Bn}₂)(H₂)]BAR^F₄, [1-H₂]⁺BAR^F₄. Density functional (DFT) calculations^{28–33} were carried out on the boat–chair conformer (A) and the chair–boat conformer (C) of [1-H₂]⁺ as well as the corresponding isomers (B, D, and E) of the product of heterolytic cleavage, [1-FeH-NH]⁺ (see Scheme 7). Optimization of the boat–chair conformer (C) of [1-H₂]⁺ started from the crystal structure of [1-H₂]⁺. The optimized structure of conformer C is in good agreement with the X-ray structure (see Supporting Information for a

comparison of the selected distances and angles) with the axis of the H–H bond parallel to the P–P vector. Structure A is related to structure C by conformational changes of the two six-membered rings. The calculated structure for the chair–boat conformer A also shows the bond of the H₂ ligand is parallel to the P–P vector, and it is found to be 1.1 kcal/mol more stable than C.³⁴ The small energy difference due to ligand conformational changes is consistent with the DFT calculations on related Ni systems and also indicates that both conformers should be present in solution.

Attempts to orient the H₂ ligand so that the H–H bond was perpendicular to the P–P vector, i.e., one H atom pointing toward the pendant N base, resulted in the calculations converging to isomer B, the H₂ heterolytic cleavage product, which lies 4.72 kcal/mol above A. The energy difference suggests the intramolecular H₂ heterolytic cleavage of 1-H₂ from isomer A to B is a slightly uphill reaction but thermodynamically accessible at room temperature, as indicated by the experimentally observed H–H and D–D cleavage. The calculated ΔG[°] (4.72 kcal/mol) reflects an equilibrium constant of 0.003 between A and B at 22 °C, which explains why [1-FeH-NH]⁺ was not observed by NMR spectroscopy. The transition state for the reaction from A to B was also optimized. The energy of the transition state is 6.12 kcal/mol above A, a relatively small reaction barrier, implying a rapid proton exchange between the N of P^{Ph}₂N^{Bn}₂ and the hydride ligand. The N–H distance of 1.367 Å in the optimized structure of the transition state suggests a hydrogen bond between the N and the H₂. The H–H bond distance is about 0.89 Å for both A and C, slightly shorter than the value (0.92 Å) derived from our NMR measurements. In addition, the H–H bond is elongated to 0.99 Å in the transition-state structure compared to the values of structures A and C and lengthens further to 1.359 Å in isomer B. In isomer B the N–H distance is 1.09 Å, and the Fe–H distance is 1.538 Å, suggesting the formation of a N–H bond and an Fe–H bond as a result of the heterolytic H–H cleavage. The structure of the transition state

illustrates the role that a pendant base can play in decreasing the reaction barrier to H–H bond cleavage/formation. It is also of interest that isomers **D** and **E** are 24.71 and 17.12 kcal/mol, respectively, higher in energy than isomer **B**. The energy difference between **D** and **E** arises from the position of the Bn group at the axial vs equatorial position of the six-membered ring adjacent to the H₂. The shorter H–H and longer N–H distance suggests that the intramolecular H–H interaction considerably stabilizes isomer **B** relative to **D** and **E**. These protic–hydridic interactions (i.e., Fe–H···H–N) have been referred to as “dihydrogen bonding”.³⁵

For the sake of completeness, we also calculated the possibility of intermolecular H₂ heterolytic cleavage between two molecules of isomer **A** (see Supporting Information, Figure S30). It was found that the intermolecular reaction is uphill by 48.00 kcal/mol, ca. 11 times the barrier for the intramolecular pathway. Efforts to find a transition state for the intermolecular reaction failed; two molecules of isomer **C** cannot easily approach each other, which further suggests a low probability for an intermolecular pathway.

Electrochemical Studies. A cyclic voltammogram of **1-Cl** in fluorobenzene is shown in Figure 4a. It consists of a single reversible one-electron oxidation wave at –0.61 V vs the Cp₂Fe⁺⁰ couple. A plot of the peak current of the anodic wave vs the square root of the scan rate is linear, indicating that this

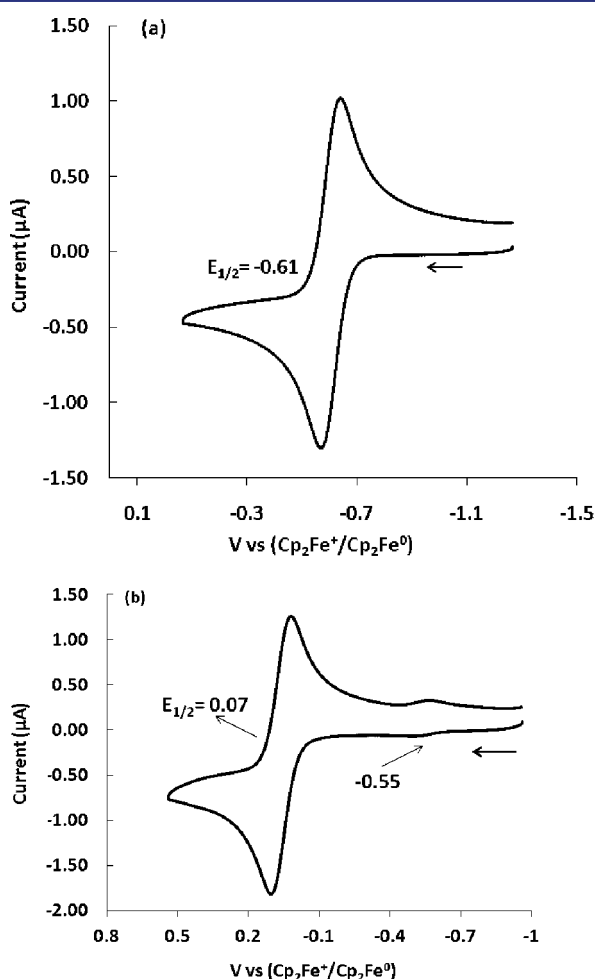


Figure 4. (a) Cyclic voltammogram of **1-Cl** (1 mM) and (b) **[1]⁺** (1 mM). Conditions: scan rate, 100 mV/s; electrolyte, 0.2 M *n*-Bu₄NB(C₆F₅)₄ in fluorobenzene.

oxidation process is under diffusion control.³⁶ This wave is assigned to the Fe^{III/II} couple of **1-Cl**. Similar reversible one-electron oxidation waves are also observed for **2-Cl** (–0.51 V, see Figure S19, Supporting Information) and **3-Cl** (–0.68 V, see Figure S20, Supporting Information).

Figure 4b shows a cyclic voltammogram recorded on a solution prepared by treating **1-Cl** in fluorobenzene with NaBAR^F₄ under an argon atmosphere. A reversible oxidation wave is observed at 0.07 V with a peak-to-peak separation (ΔE_p) of 81 mV. Under these conditions, a ΔE_p of 76 mV was observed for the Cp₂Fe⁺/Cp₂Fe couple. The scan rate dependence of the peak current indicates that this oxidation is diffusion controlled.³⁶ This redox process is assigned to the oxidation/reduction of the coordinatively unsaturated 16-electron species [CpFe(P^{Ph}₂N^{Bn}₂)]⁺, **[1]⁺**. The analogous [Cp*Fe(dppe)]⁺ complex has been reported to have a reversible oxidation wave at –0.29 V vs the Cp₂Fe⁺/Cp₂Fe couple in tetrahydrofuran.³⁷ A smaller wave is also observed at –0.55 V that is currently unassigned. There are also two irreversible reduction waves for **[1]⁺** with peaks at –1.54 and –1.80 V at 100 mV/s scan rate (see Figure S24, Supporting Information).

Figure 5 shows cyclic voltammograms of complex **[1-H₂]⁺** recorded in fluorobenzene under H₂ (1.0 atm). The black trace

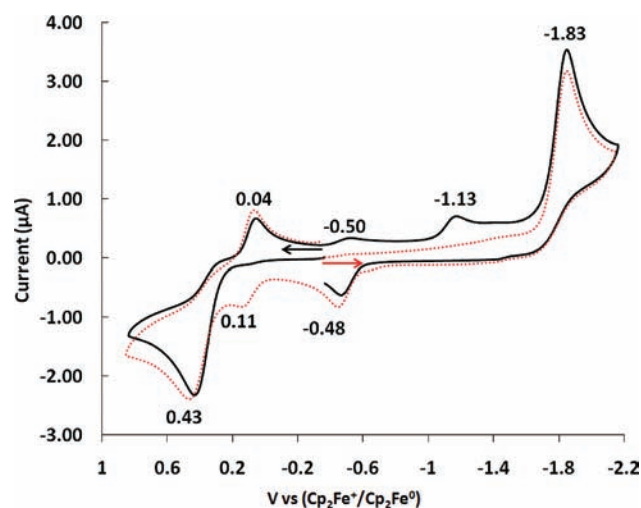


Figure 5. Cyclic voltammograms of **[1-H₂]⁺** in fluorobenzene. For the black trace (solid line), the initial scan direction was positive. For the red trace (dotted line), the initial scan direction was negative. Conditions: 1.0 mM **[1-H₂]⁺**; scan rate, 100 mV/s; electrolyte, 0.2 M *n*-Bu₄NBAR^F₄; 1.0 atm H₂.

shows a cyclic voltammogram in which the initial scan direction is positive. An irreversible oxidation wave is observed with an anodic peak potential of 0.43 V. This wave becomes partially reversible at higher scan rates (Figure S21, Supporting Information); it is assigned to the oxidation of **[1-H₂]⁺** (Fe^{II}) to **[1-H₂]²⁺** (Fe^{III}) followed by loss of H₂. In support of this interpretation, a wave is observed at 0.07 V (average of oxidation and reduction peaks, see Figure S23, Supporting Information) on the return scan, identical to the potential observed for the coordinatively unsaturated 16-electron species [CpFe(P^{Ph}₂N^{Bn}₂)]⁺, **[1]⁺**, discussed above. The small waves at –0.50 and –1.13 V, which are related to the oxidation at 0.43 V and the reduction at –1.83 (see below), are unassigned. When

initial scan direction is negative, the waves at -0.50 and -1.13 V are not observed. The dotted red trace in Figure 5 is a cyclic voltammogram for which the initial scan direction is negative. In this case, an irreversible reduction wave is observed with a peak potential of -1.83 V that is assigned to the $\text{Fe}^{\text{II/I}}$ couple corresponding to the reduction of $[\text{1-H}_2]^+$ to $[\text{1-H}_2]$, followed by hydrogen loss. Again on the return scan, the oxidation wave at 0.07 V of $[\text{1}]^+$ is associated with the reduction wave at -1.83 V, consistent with H_2 loss following reduction.

The cyclic voltammogram of **1-H** shows an irreversible oxidation at -0.72 V at a scan rate of 0.1 V/s (see Figure 6a) as

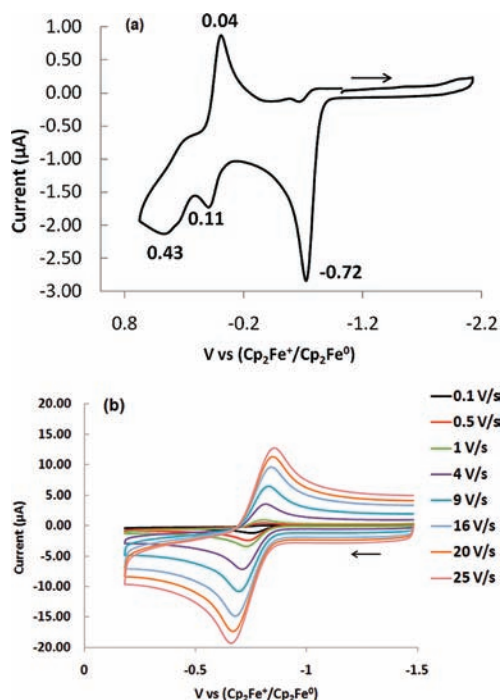


Figure 6. (a) Cyclic voltammogram of **1-H** (1.0 mM solution). Conditions: scan rate, 100 mV/s; electrolyte, 0.2 M $n\text{-Bu}_4\text{NBAR}_4^{\text{F}}$ in PhF; under Ar (1.0 atm). (b) The oxidation wave at -0.72 V recorded at scan rates from 0.1 – 25 V/s.

well as waves at 0.11 and 0.43 V that correspond to the oxidation of $[\text{1}]^+$ and $[\text{1-H}_2]^+$, respectively. The $\text{Fe}^{\text{III/II}}$ redox couples for the series **1-H** (-0.72 V), **1-Cl** (-0.61 V) and $[\text{1-H}_2]^+$ (0.43 V) follow the order of Lever's³⁸ electrochemical parameters for the ligands H^- (-0.4 V), Cl^- (-0.24 V), and H_2 (0.8 V).³⁹ In addition, the peak current of the irreversible oxidation wave at -0.72 V is almost the same as that observed for the oxidation wave of **1-Cl** under identical conditions and at the same concentration. This indicates that the oxidation of **1-H** at -0.72 V is an one-electron process. The oxidation of **1-H** becomes more reversible at higher scan rates (see Figure 6b), as indicated by the associated return reduction wave with a peak at

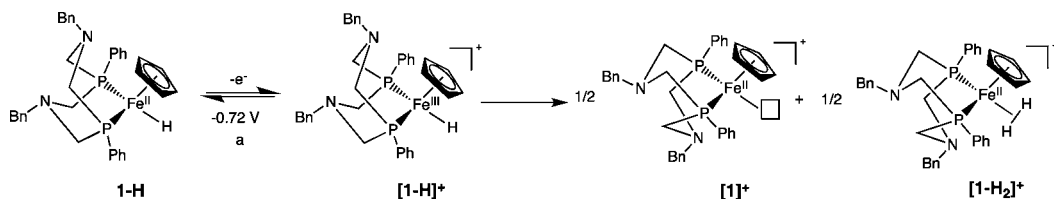
-0.78 V, and at a scan rate of 25 V/s, the ratio of the cathodic current to the anodic current, i_c/i_a , is 0.98 . In addition to the irreversible oxidation wave at -0.72 V, an oxidation wave is observed at 0.11 V with an associated reduction at 0.04 V that is assigned to the formation of $[\text{1}]^+$ as discussed above. A second irreversible oxidation wave is observed at $+0.43$ V that is assigned to $[\text{1-H}_2]^+$. These two new oxidation waves are half the height of the oxidation wave. These data are consistent with the reactions shown in Scheme 8. The oxidation of **1-H** forms $[\text{1-H}]^+$, which reacts with a second molecule of $[\text{1-H}]^+$ to form $[\text{1}]^+$ and $[\text{1-H}_2]^+$. This scheme illustrates the overall stoichiometry of the reactions but is not meant to imply a mechanism.

Complex **2-H** shows similar electrochemical behavior to **1-H**, as shown in Figure S27, Supporting Information, but the oxidation of **2-H** to 2-H^+ is somewhat more reversible than for **1-H**, as indicated by some reversibility of the $2\text{-H}^+/2\text{-H}$ couple ($E_{1/2} = -0.65$ V) even at 100 mV/s. Complex **3-H-a** exhibits an irreversible oxidation at -0.82 V. This is a somewhat unexpected observation, because $\text{Cp}^*\text{Fe}(\text{dppe})\text{H}$ is reported to have a reversible oxidation at -0.75 V at a scan rate of 1.0 V/s.³⁷ At scan rates above 9 V/s, the oxidation of **3-H-a** is quasireversible as a cathodic wave can be clearly observed (see Figure S28, Supporting Information). At 25 V/s, the i_c/i_a is ca. 0.3 . These electrochemical data suggest **3-H-a** undergoes a faster chemical process following the electron transfer step than either **1-H** or **2-H**. The irreversibility may be due to an increased ring strain for **3-H** compared to **1-H** and **2-H**, as suggested by smaller P–Fe–P angles for **3-Cl** compared to **1-Cl** and **2-Cl**.

Cyclic voltammograms of **1-H** in fluorobenzene solutions titrated with increasing amounts of DBU are shown in Figure 7. The addition of 5 equiv of base results in an increase in the current observed for oxidation wave at -0.72 V by a factor of 2.1 – 2.4 . The increase in current observed for the oxidation wave at -0.72 V implies that a second electron transfer event becomes possible in the presence of base, likely as a result of fast deprotonation of $[\text{CpFe}^{\text{III}}(\text{P}^{\text{Ph}}_2\text{N}^{\text{Bn}}_2)(\text{H})]^+$, $[\text{1-H}]^+$, to form $[\text{CpFe}^{\text{I}}(\text{P}^{\text{Ph}}_2\text{N}^{\text{Bn}}_2)]$. This Fe^{I} species should be readily oxidized at -0.72 V resulting in an ECE reaction as shown in the first three steps of Scheme 9.

Addition of H_2 to this solution did not result in any further increase in current. These results indicate that catalytic oxidation of H_2 is not occurring. Consistent with this interpretation, chemical oxidation of **1-H** using Cp_2Fe^+ in the presence of DBU and D_2 does not result in the formation of sufficient DBU- D^+ to indicate a catalytic reaction. In addition, when $[\text{1}]^+$ is generated by reaction of **1-Cl** with $\text{NaBAR}_4^{\text{F}}$ and treated with DBU, a single new resonance is observed at 46.4 ppm in the $^{31}\text{P}\{\text{1H}\}$ NMR spectrum. This reaction is accompanied by a color change from dark brown to pink. Upon addition of DBU, the oxidation wave at 0.07 V observed for $[\text{1}]^+$ shifts to -0.05 V, and the reduction waves at 1.54 and 1.80 V disappear, consistent with the formation of a new species (see Figure S25, Supporting Information). Based on

Scheme 8



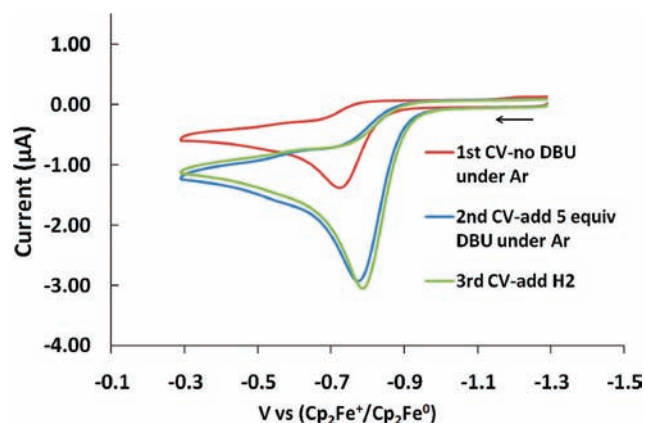


Figure 7. Cyclic voltammogram of **1-H** (0.5 mM) in the absence of DBU (red trace), in the presence of DBU (5 equiv, blue trace), and in the presence of DBU (5 equiv) and H_2 (1.0 atm, green trace). Conditions: scan rate, 100 mV/s; electrolyte, 0.2 M $n\text{-Bu}_4\text{NBAR}^{\text{F}_4}$ in PhF.

these data, the new species is tentatively identified as $[\mathbf{1}(\text{DBU})]^+$, in which DBU has coordinated to iron to form an 18-electron complex (reaction C_2 of Scheme 9). There are a few examples of metal complexes that have DBU as a ligand.⁴⁰ Upon treatment of $[\mathbf{1}(\text{DBU})]^+$ with H_2 , no $[\mathbf{1}\text{-H}_2]^+$ or **1-H** was formed. However, addition H_2 to $[\mathbf{1}]^+$ followed by DBU led to the immediate formation of **1-H**. It can be deduced that formation of $[\mathbf{1}(\text{DBU})]^+$ upon oxidation of **1-H** under H_2 in the presence of DBU would effectively limit catalysis, as observed. Similar results were obtained for **2-H** and **3-H**.

DISCUSSION

A series of new CpFe derivatives containing the $\text{P}^{\text{Ph}}_2\text{N}^{\text{R}}_2$ ligands ($\text{R} = \text{Ph}, \text{Bn}$) and the base-free $\text{P}^{\text{Ph}}_2\text{C}_5$ ligand have been synthesized and characterized by X-ray diffraction, electrochemical, and spectroscopic techniques. The features of primary interest in this study are characteristics of the complexes that are relevant to the development of electrocatalytic activity for H_2 oxidation or formation. These include the conformations of the ligand chelate rings and the positioning of the amine bases relative to the active coordination site at iron, the ability of the complexes to coordinate and effect heterolytic cleavage of H_2 , and the role of the pendant

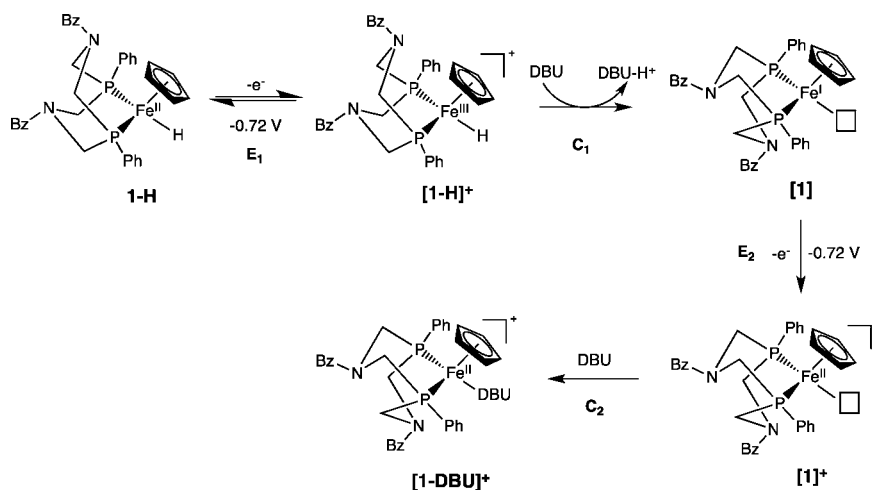
bases in facilitating proton transfer between the metal center and the solution.

The structures of all of the $[\text{CpFe}(\text{P}_2\text{N}_2)\text{L}]^{n+}$ complexes reported in this study have diphosphine ligands with one six-membered chelate ring in a boat conformation and the other in a chair conformation. This is the most common conformational arrangement observed for other complexes with this class of ligand as well. If the ligand L bears a formal negative charge, such as chloride or hydride, then the interaction between the N atom of the diphosphine ligand and this ligand is repulsive. This results in a chair conformation for this chelate ring to minimize the interaction and a boat conformation for the ring adjacent to the Cp ligand. However, for the complex with a CO ligand, $[\mathbf{1}\text{-CO}]^+$, there is an attractive interaction between the nitrogen lone pair and the partial positive charge on the carbonyl carbon, as indicated by the short $\text{N}\cdots\text{C}$ distance (2.85 Å) that is significantly less than the sum of the van der Waals radii. Similar, but much weaker, $\text{N}\cdots\text{CO}$ interactions were reported previously for $\text{Mn}(\text{P}^{\text{Ph}}_2\text{N}^{\text{Bn}}_2)(\text{dppm})(\text{CO})(\text{H})$ (where dppm is 1,2-bis(diphenylphosphino)methane, $\text{N}\cdots\text{C} = 3.17$ Å)⁴¹ and $[\text{Ni}(\text{P}^{\text{Ph}}_2\text{N}^{\text{Bn}}_2)_2(\text{CO})](\text{BF}_4)_2$ ($\text{N}\cdots\text{C}$ distances of 3.30 and 3.38 Å for both $\text{P}^{\text{Ph}}_2\text{N}^{\text{Bn}}_2$ ligands).⁴² The much shorter $\text{N}\cdots\text{C}$ distance observed for $[\mathbf{1}\text{-CO}]^+$ implies a stronger interaction. Complex $[\mathbf{1}\text{-CO}]^+$ is also of interest because it suggests an arrested nucleophilic attack on the coordinated CO ligand, related to previously reported nucleophilic attacks of primary amines on coordinated CO.⁴³

Morris^{18,19} and Heinekey¹⁷ have shown that the value of J_{HD} is correlated with the H–D distance of the bound HD ligand, with smaller J_{HD} values indicating longer H–D distances. The J_{HD} value of 25 Hz that we found in $[\text{CpFe}(\text{P}^{\text{Ph}}_2\text{C}_5)(\text{HD})]^+$ is smaller than those reported for other $\text{Fe}(\text{H}_2)^+$ complexes. Morris and co-workers found $J_{\text{HD}} = 32$ Hz for $[\text{Fe}(\text{HD})(\text{H})(\text{dppe})_2]^+$.⁴⁴ A slightly smaller J_{HD} of 29.8 Hz was found in the related water-soluble iron complex $[\text{Fe}(\text{HD})(\text{H})(\text{DMeOPrPE})_2]^+$ ($\text{DMeOPrPE} = 1,2\text{-bis}(\text{bis}(\text{methoxypropyl})\text{-phosphino})\text{ethane}$) studied by Tyler and co-workers.⁴⁵ A small J_{HD} value of 27 Hz was reported for $[\text{Cp}^*\text{Fe}(\text{dppe})(\text{HD})]^+$.⁴⁶

For the dihydrogen complex $[\mathbf{1}\text{-H}_2]^+$, the energies of the chair/boat conformations of the chelate rings appear to be nearly balanced. A crystal structure determination indicates that the six-membered ring adjacent to the H_2 ligand adopts a chair conformation, while DFT calculations suggest that in solution the boat conformation is more stable. For the latter

Scheme 9



conformation, the pendant base is positioned to participate in H₂ cleavage with a low activation energy.

Each of the complexes **1-Cl**, **2-Cl**, and **3-Cl** undergoes chloride abstraction under 1.0 atm of H₂ in fluorobenzene to rapidly form the corresponding dihydrogen complex. Further studies with a mixture of H₂ and D₂ provide a method to evaluate activity for heterolytic cleavage of H₂. The hydrogenase enzymes⁴⁷ have been shown to undergo exchange reactions to produce HD under an H₂/D₂ atmosphere. Diiron model compounds reported by Darensbourg and co-workers⁴⁸ show H₂/D₂ scrambling but involves photolytically induced CO loss, so it is significantly different than the reactivity of the enzyme and the Fe complexes reported here. Exposure of the dihydrogen complexes prepared in this study to mixtures of D₂ and H₂ gas results in the exchange of the H₂ ligand with D₂ for all three complexes. However, only complexes [1-H₂]⁺ and [2-H₂]⁺ with the P₂N₂ ligands exhibited H/D exchange to form HD gas and coordinated HD, detected over a period of minutes. The relatively rapid H/D exchange observed for [1-H₂]⁺ and [2-H₂]⁺ is consistent with intramolecular heterolytic cleavage of H₂ to form [1-FeH-NH]⁺ and [2-FeH-NH]⁺ as intermediates. This rapid heterolytic cleavage, followed by proton transfer between species in solution, leads to the observed H/D exchange.

Our experimental results are supported by DFT calculations that suggest the barrier (ΔG^\ddagger) and the free energy (ΔG°) of heterolytic H-H cleavage are small ($\Delta G^\ddagger = 6.12$ and $\Delta G^\circ = 4.72$ kcal/mol). DFT calculations on the diiron (Fe^{II}) active site model reported by Hall et al. indicate that the bridging di(thiomethyl)amine ligand can facilitate heterolytic H-H bond cleavage with comparable free energies, $\Delta G^\ddagger = 4.9$ and $\Delta G^\circ = 3.5$ kcal/mol.⁷ Both calculations also reveal almost identical reaction coordinates for H-H cleavage. As sketched in Scheme 7 (and Figure 1 in ref 7), the H-H bond length gradually increases from 0.89 Å for the dihydrogen complex to 0.99 Å for the transition state and finally to 1.36 Å for the H₂ heterolytic cleavage product. This increase in the H-H distance is accompanied by the disappearance of Fe-(H₂) σ bond and the formation of Fe-H and N-H bonds as well as an Fe-H...H-N "dihydrogen bond" in the transition-state structure and the heterolytic cleavage product. As displayed in Schemes 5 and 7 and the calculations from Hall,⁷ the fundamental requirements for heterolytic H₂ cleavage at the active site of [FeFe]-hydrogenases and synthetic catalysts based on Fe are: (1) a ferrous (Fe^{II}) center for H₂ bonding and activation; (2) a pendant amine base for H-H bond cleavage; and (3) energy matching of the hydride acceptor abilities of the Fe and the proton acceptor abilities of the pendant amine. Therefore, complexes [1-H₂]⁺ and [2-H₂]⁺ with positioned pendant amines serve as models of the distal Fe site coordinated with the H₂ ligand of the enzymatic active site, suggesting mononuclear Fe complexes can be competent models of the active site of [FeFe]-hydrogenase enzymes.

In contrast to [1-H₂]⁺ and [2-H₂]⁺, [3-H₂]⁺ with no pendant amines exhibited no detectable H/D exchange after 19 h, although slow exchange was observed for this complex in the presence of two equivalents of an external base, such as aniline or benzylamine. The heterolytic cleavage of H₂ and proton transfer to solution observed for the complexes with the pendant amines, [1-H₂]⁺ and [2-H₂]⁺, suggest that complexes containing positioned pendant amines are likely to promote higher catalytic activity for H₂ oxidation than systems that lack these proton relays.

All three of the dihydrogen complexes can be deprotonated by the base DBU ($pK_a = 24$ for H-DBU⁺ in CH₃CN)²⁰ to form the corresponding hydride derivatives **1-H**, **2-H**, and **3-H**. Deprotonation with excess triethylamine ($pK_a = 18.8$ for H-NEt₃⁺ in CH₃CN)²⁰ is not observed, and this brackets the effective pK_a of the coordinated H₂ ligand in this series in the range of 20–24 in acetonitrile. As noted before, our experiments were conducted in fluorobenzene since the complexes react with CH₃CN, but the comparison of pK_a values cited are for CH₃CN solvent. These complexes are less acidic than previously reported cationic iron dihydrogen complexes reported by Morris and co-workers, such as *trans*-[Fe(H₂)H(dppe)₂]BPh₄ (pK_a in CH₃CN estimated as 18.39 based on measurements in THF).⁴⁹

Electrochemical oxidation of **1-H** produces [1-H₂]⁺ and [1]⁺, as shown in Scheme 8. Paramagnetic complexes similar to [1]⁺, [Cp*Fe(dppe)]⁺²⁶ and [Cp*Fe(dippe)]⁺²⁷ (dippe = 1,2-bis-(diisopropylphosphino)ethane), have been crystallographically characterized. However, in the presence of a base, such as DBU, [1-H]⁺ is deprotonated (step C₁ of Scheme 9), followed by a second electron transfer reaction (step E₂). Coordination of H₂ would lead to regeneration of [1-H₂]⁺ and completion of a catalytic cycle. However, H₂ binding to [1]⁺ is not competitive with the coordination of DBU, which is present in solution in a relatively high concentration. The preferential coordination of base rather than H₂ prevents the completion of the desired cycle, and catalysis is not observed for **1-H**. Similar inhibition by base is also observed for **2-H** and **3-H**. Although we have not yet found conditions for which **1-H** is an electrocatalyst for oxidation of H₂, this complex does meet important requirements for catalytic activity, including rapid binding and heterolytic activation of H₂, followed by proton transfer to solution. The results presented here suggest a rationale for designing related iron derivatives with bulky ligands and appropriate pK_a values to favor coordination and heterolytic cleavage of H₂ in the presence of a less coordinating base. Our studies of such ligand modifications and their impact on catalytic activity for H₂ oxidation will be reported.

SUMMARY AND CONCLUSIONS

A series of new CpFe(diphosphine)H, [CpFe(diphosphine)-(H₂)]BAR₄^F, and related complexes have been prepared containing P^{Ph}₂N^{Bn}₂ and P^{Ph}₂N^{Ph}₂ ligands with pendant amines to explore the utility of this structural motif for developing electrocatalysts for H₂ oxidation and production. Based on the structural studies of several of these complexes and DFT calculations, it is concluded that attractive or repulsive interactions between the sixth ligand and the pendant amine of the adjacent six-membered ring of the cyclic diphosphine determine the conformations adopted by these ligand chelate rings. An attractive interaction between the H₂ ligand in [1-H₂]⁺BAR₄^F and [2-H₂]⁺BAR₄^F and the pendant base of the diphosphine ligand facilitates the intramolecular heterolytic cleavage of H₂. Rapid H/D exchange is observed for these complexes under an H₂/D₂ atmosphere, whereas under the same conditions HD formation is not observed for [3-H₂]⁺BAR₄^F, which does not have a base incorporated in its second coordination sphere. Together with the DFT calculations, the experimental observations indicate crucial structural features for the intramolecular heterolytic cleavage of H₂ are a ferrous (Fe^{II}) center, a pendant amine, and matched hydride and proton acceptor abilities.

All of the cationic dihydrogen complexes, [1-H₂]⁺BAR₄^F, [2-H₂]⁺BAR₄^F, and [3-H₂]⁺BAR₄^F, can be deprotonated by DBU

to form the corresponding neutral hydrides. Electrochemical studies have shown that oxidation of **1-H** in the presence of DBU as a base results in the electrochemical and chemical steps required for a catalytic system (see Scheme 9); however, preferential binding of DBU rather than H_2 at the vacant coordination site of $[CpFe(P^{Ph}_2N^{Bn}_2)]BAR^F_4$, $1^+-BAR^F_4$, prevents the completion of a catalytic cycle. Rational catalyst design will involve further synthetic modifications to control the steric bulk of the ligands on the iron complex, the redox potential of the catalyst, and the acidity of the coordinated H_2 molecule in order to achieve active molecular electrocatalysts for H_2 oxidation based on iron.

EXPERIMENTAL SECTION

General Experimental Procedures. 1H , 2H , ^{15}N , and ^{31}P NMR spectra were recorded on a Varian Inova spectrometer (500 MHz for 1H) at 20 °C unless otherwise noted. All 1H chemical shifts have been internally calibrated to the monoprotio impurity of the deuterated solvent. The 2H NMR spectra were internally calibrated to the deuterated solvent. The ^{31}P NMR spectra were proton decoupled and referenced to external phosphoric acid.

Electrochemical experiments were carried out under an atmosphere of argon, or hydrogen when indicated, in fluorobenzene solutions containing 0.2 M $n-Bu_4NB(C_6F_5)_4$. Cyclic voltammetry experiments were carried out with a CH Instruments model 660C potentiostat. The working electrode (1 mm PEEK-encased glassy carbon, Cypress Systems EE040) was polished using Al_2O_3 (BAS CF-1050, dried at 150 °C under vacuum), suspended in acetonitrile, and then rinsed with neat PhF. A glassy carbon rod (Structure Probe, Inc.) was used as the counter electrode, and a silver wire suspended in a solution of 0.2 M $n-Bu_4NB(C_6F_5)_4$ in PhF and separated from the analyte solution by a Vycor frit was used as the pseudoreference electrode. Cobaltocenium hexafluorophosphate (Cp_2CoPF_6) or bis(pentamethylcyclopentadienyl)iron (Cp^*_2Fe) was used as an internal standard, and all potentials are referenced to the $Cp_2Fe^{+/0}$ couple at 0 V.

X-ray Structures. For all reported structures, a 10× microscope was used to identify suitable crystals of the same habit. Each crystal was coated in Paratone, affixed to a nylon loop and placed under streaming nitrogen (100 K) in a Bruker KAPPA APEX II CCD diffractometer with 0.71073 Å Mo $K\alpha$ radiation (see details in cif files in the Supporting Information). The space groups were determined on the basis of systematic absences and intensity statistics. The structures were solved by direct methods and refined by full-matrix least-squares on F^2 . Anisotropic displacement parameters were determined for all nonhydrogen atoms. Hydrogen atoms were placed at idealized positions and refined with fixed isotropic displacement parameters. Disorder fragments (i.e., the disordered cocrystallized ether in structure of $[CpFe(P^{Ph}_2N^{Bn}_2)(CO)]Cl$, $[1-CO]Cl$, and the disordered BAR^F_4 anion of $[CpFe(P^{Ph}_2N^{Bn}_2)(H_2)]BAR^F_4$, (**1-H₂**) was modeled using appropriate restraints and constraints. The H_2 ligand of $[1-H_2]^+$ cannot be accurately located using X-ray diffraction data; the single residue ca. 1.60 Å from the Fe atom was modeled and refined as an H_2 ligand. Programs used were: data reduction, SAINTPLUS, version 6.63;⁵⁰ absorption correction, SADAB;⁵¹ structural solution, SHELXS-97;⁵² structural refinement, SHELXL-97;⁵³ graphics, Ortep-3(V2) for Windows.⁵⁴ Crystallographic information (available as electronic files cif format) is provided in the Supporting Information.

Synthesis and Materials. All reactions and manipulations were conducted under a N_2 , Ar, or H_2 atmosphere using standard Schlenk techniques or a glovebox. Solvents were dried using an activated alumina column. All NMR solvents were purified according to standard methods. Photolysis reactions were conducted using a water-jacketed medium pressure mercury lamp (Ace Hanovia 450 W). Quartz glassware was used for all photolysis reactions. $[CpFe(CO)_2Cl]$,⁵⁵ 1,3-diphenyl-5,7-dibenzyl-1,5-diaza-3,7-diphosphacyclooctane ($P^{Ph}_2N^{Bn}_2$ and $P^{Ph}_2^{15}N^{Bn}_2$),⁵⁶ 1,3,5,7-tetraphenyl-1,5-diaza-3,7-diphosphacyclooctane ($P^{Ph}_2N^{Ph}_2$),⁵ 1,5-diphenyl-1,5-diphosphocane ($P^{Ph}_2C_6$),²³ and 1,4-diphenyl-1,4-diphosphoheptane ($P^{Ph}_2C_5$)²⁴ were

prepared according to published procedures. All other reagents were used as received.

Computational Details. Molecular structures were optimized using DFT theory with the hybrid B3P86²⁸ exchange and correlation functional using the Stuttgart–Dresden relativistic ECP and associated basis set (SDD) for Fe⁵⁹ and 6-31G** for all nonmetal atoms.³⁰ Harmonic vibrational frequencies were calculated at the optimized geometries using the same level of theory to estimate the zero-point energy (ZPE) and the thermal contributions (298 K and 1.0 atm) to the gas-phase free energy. Free energies of solvation in toluene were then computed using the conductor-like polarizable continuum model (CPCM)³¹ with Bondi radii.³³ All calculations were carried out with Gaussian 09.³²

$CpFe(P^{Ph}_2N^{Bn}_2)Cl$, (1-Cl**).** $[CpFe(CO)_2Cl]$ (0.440 g, 2.07 mmol) and $P^{Ph}_2N^{Bn}_2$ (1.000 g, 2.07 mmol) were dissolved in toluene (150 mL) in a 250 mL quartz flask. The solution was photolyzed for approximately 48 h. The solution gradually changed from red to black, with concomitant formation of a yellow precipitate, $[CpFe(P^{Ph}_2N^{Bn}_2)(CO)]Cl$, $[1-CO]Cl$. The reaction was complete when the yellow intermediate, $[1-CO]Cl$, disappeared, which was further confirmed by IR and ^{31}P NMR spectroscopy. The resulting black solution was filtered through Celite to remove insoluble residues, and the filtrate was evaporated under vacuum to give a black solid. Recrystallization of the crude product from 20 mL of PhF layered with 200 mL of hexane yielded 1.07 g (81%) of black crystals suitable for X-ray diffraction. Anal. calcd. for $C_{35}H_{37}N_2FeP_2Cl$: C, 65.79; H, 5.84; N, 4.38. Found: C, 65.75; H, 5.77; N, 4.59. 1H NMR (CD_2Cl_2): δ 7.95 (m, 4 H, $CH_2C_6H_5$), 7.47 (m, 6 H, $CH_3C_6H_5$), 7.20 (m, 10 H, PC_6H_5), 3.97 (s, 5 H, C_5H_5), 3.86 (s, 2 H, $NCH_2C_6H_5$), 3.50 (s, 2 H, $NCH_2C_6H_5$), 3.38 (dt, $J_{HH} = 12.8$ Hz, $J_{PH} = 5.6$ Hz, 2 H, NCH_2P), 3.16 (d, $J_{HH} = 12.8$ Hz, 2 H, NCH_2P), 3.03 (d, $J_{HH} = 11.9$ Hz, 2 H, NCH_2P), 2.52 (dt, $J_{HH} = 11.9$ Hz, $J_{PH} = 8.3$ Hz, 2 H, NCH_2P). $^{31}P\{^1H\}$ NMR (CD_2Cl_2): δ 57.2 (s).

$[CpFe(P^{Ph}_2N^{Bn}_2)(CO)]Cl$, $[1-CO]Cl$. The yellow precipitate that formed in the photolytic preparation of $[CpFe(P^{Ph}_2N^{Bn}_2)Cl]$ described above was separated by filtration, washed with toluene, and dried under vacuum to give a yellow powder (0.028 g, 20% based on 0.060 g $[CpFe(CO)_2Cl]$). Single crystals suitable for X-ray diffraction were grown from a CH_2Cl_2 solution layered with hexane. Anal. calcd. for $C_{35}H_{37}N_2FeP_2Cl$: C, 64.83; H, 5.59; N, 4.20. Found: C, 64.15; H, 5.33; N, 4.68. IR (ν (CO), CH_2Cl_2 , cm^{-1}): 1964. 1H NMR (CD_2Cl_2): δ 7.50 (m, 10 H, $CH_2C_6H_5$), 7.35 (m, 8 H, $CH_2C_6H_5$), 7.25 (m, 2 H, PC_6H_5), 4.69 (s, 5 H, C_5H_5), 4.08 (s, 2 H, $NCH_2C_6H_5$), 3.90 (d, 2 H, $J_{HH} = 13$ Hz, NCH_2P), 3.81 (s, 2 H, $NCH_2C_6H_5$), 3.42 (dt, $J_{PH} = 5$ Hz, $J_{HH} = 13$ Hz, 2 H, NCH_2P), 3.05 (dt, $J_{PH} = 4$ Hz, $J_{HH} = 13$ Hz, 2 H, NCH_2P), 2.86 (d, $J_{HH} = 13$ Hz, 4.01 H, NCH_2P). $^{31}P\{^1H\}$ NMR (CD_2Cl_2): δ 52.7 (s).

Generation of $[CpFe(P^{Ph}_2N^{Bn}_2)]BAR^F_4$ ($1^+-BAR^F_4$) and $CpFeP^{Ph}_2N^{Ph}_2]BAR^F_4$ ($2^+-BAR^F_4$). Under Ar, a mixture of $NaBAR^F_4$ (0.018 g, 0.020 mmol) and **1-Cl** (0.013 g, 0.020 mmol) (or **2-Cl**) was dissolved in 1 mL of fluorobenzene (PhF) and stirred for 0.5 h to give a dark-brown solution of $1^+-BAR^F_4$ (or $2^+-BAR^F_4$). This solution prepared in situ was used for reactions or cyclic voltammetry (CV) studies. ESI-MS (e/z) for 1^+ : observed at 603.1785, predicted at 603.1782.

$[CpFe(P^{Ph}_2N^{Bn}_2)(H_2)]BAR^F_4$, $[1-H_2]^+$. Under an atmosphere of H_2 (1.0 atm), a solution of $[CpFe(P^{Ph}_2N^{Bn}_2)Cl]$ (0.128 mg, 0.200 mmol) in 5 mL of PhF was added via cannula to solid $NaBAR^F_4$ (sodium tetrakis[3,5-bis(trifluoromethyl)phenyl]borate) (0.180 g, 0.200 mmol). The mixture was stirred for 15 min, leading to a color change from black to yellow. The workup was carried out under an argon atmosphere in a glovebox. After filtration through Celite, 30 mL of hexane was added to precipitate the product as a yellow solid (0.230 g, 80%). $[CpFe(P^{Ph}_2N^{Bn}_2)(H_2)]BAR^F_4$ is stable under H_2 at room temperature for several weeks. $[1-H_2]^+$ can also be prepared by addition of H_2 to $1^+-BAR^F_4$. Anal. calcd. for $C_{67}H_{51}BN_2F_{24}FeP_2$: C, 54.79; H, 3.50; N, 1.91. Found: C, 54.77; H, 3.46; N, 1.86. 1H NMR ($PhCl-d_5$): δ 8.02 (s, 8 H, $B(C_6F_5)_3$), 7.34 (s, 4 H, $B(C_6F_5)_3$), 7.03 (m, 8 H, C_6H_5), 6.96 (m, 10 H, C_6H_5), 6.72 (d, 2 H, C_6H_5), 3.75 (s, 5 H, C_5H_5), 3.41 (s, 2 H, $NCH_2C_6H_5$), 3.04 (s, 2 H, $NCH_2C_6H_5$),

2.85 (dt, $J_{\text{HH}} = 15$ Hz, $J_{\text{PH}} = 5$ Hz, 2 H, NCH_2P), 2.75 (d, 2 H, $J_{\text{HH}} = 10$ Hz NCH_2P), 2.39 (dt, $J_{\text{HH}} = 15$ Hz, $J_{\text{PH}} = 5$ Hz, 2 H, NCH_2P), 1.74 (d, $J_{\text{HH}} = 15$ Hz, 2 H, NCH_2P), -12.64 (s, 2.00 H, FeH_2). $^{31}\text{P}\{^1\text{H}\}$ NMR (PhCl-d_3): δ 58.4 (s).

[CpFe(P^{Ph}₂N^{Bn})₂(HD)]BAR^F₄ ([1-HD]⁺). 1-Cl (0.013 g, 0.020 mmol) and NaBAR^F₄ (0.022, 0.024 mmol) were dissolved in 0.6 mL of PhCl-d_3 in a J. Young NMR tube under Ar. The solution was frozen using liquid N₂, and the tube was evacuated. The NMR tube was refilled with HD gas (1.0 atm). After warming to room temperature, the reaction was monitored by ¹H NMR spectroscopy. ¹H NMR (PhCl-d_3): δ -12.71 (t, $J_{\text{HD}} = 30$ Hz, 1 H, Fe(HD)).

CpFe(P^{Ph}₂N^{Bn})₂(H), (1-H). Method A. A mixture of [CpFe(P^{Ph}₂N^{Bn})₂Cl] (0.255 g, 0.400 mmol) and 3 equiv of LiAlH₄ (ca. 0.046 g) in 20 mL of THF was stirred at 22 °C for 1 h, resulting in a color change from black to orange. THF was removed by evaporation to give an orange residue. The orange residue was extracted with 20 mL of toluene. After filtration, water was added dropwise to the filtrate to quench any remaining LiAlH₄ until no further gas evolution was observed. The precipitate was removed by filtration. The solvent was evaporated, and the orange powder was dried under vacuum to give analytically pure product (0.140 g, 61%). Single crystals suitable for an X-ray diffraction study were grown from an ether solution at -35 °C. Anal. calcd. for C₃₅H₃₈N₂FeP₂: C, 69.54; H, 6.34; N, 4.63. Found: C, 69.26; H, 6.28; N, 4.63. ¹H NMR (THF-*d*₈): δ 7.58 (br, 4 H, C₆H₅), 7.44 (d, 2 H, C₆H₅), 7.30 (m, 10 H, C₆H₅), 7.19 (m, 4 H, C₆H₅), 4.00 (s, 2H, $\text{NCH}_2\text{C}_6\text{H}_5$), 4.23 (s, 5 H, C₅H₅), 3.49 (s, 2 H, $\text{NCH}_2\text{C}_6\text{H}_5$), 3.20 (d, $J_{\text{HH}} = 15$ Hz, 2 H, NCH_2P), 2.98 (m, 4 H, NCH_2P), 2.13 (d, $J_{\text{HH}} = 15$ Hz, 2 H, NCH_2P), -16.0 (t, $J_{\text{PH}} = 60$ Hz, 1 H, FeH). $^{31}\text{P}\{^1\text{H}\}$ NMR (THF-*d*₈): δ 71.8 (s).

Method B. 1,8-Diazabicyclo[5.4.0]undec-7-ene (DBU, 74 μL , 0.075 g, 0.48 mmol, ca. 1.2 equiv) was added dropwise to a solution of [CpFe(P^{Ph}₂N^{Bn})₂(H₂)]BAR^F₄ ([1-H₂]⁺) (generated in situ from 1-Cl (0.255 g, 0.400 mmol) in 10 mL of PhF. The reaction was monitored by ³¹P NMR spectroscopy to determine when it had reached completion. After removal of solvent, extraction with 30 mL of hexane yielded an orange powder (0.048 g, 20%). Its identity was confirmed by ¹H NMR and $^{31}\text{P}\{^1\text{H}\}$ NMR.

Reaction of [CpFe(P^{Ph}₂N^{Bn})₂BAR^F₄ (1⁺-BAR^F₄) with DBU. 1⁺-BAR^F₄ was generated in situ from NaBAR^F₄ (0.018 g, 0.020 mmol) and 1-Cl (0.013 g, 0.020 mmol) in 0.5 mL PhCl-d_3 in a NMR tube. Addition of DBU (6 μL , 0.040 mmol, ca. 2 equiv) to the dark-brown solution led to an immediate color change to pink. The resultant species showed a resonance at δ 46.4 in the $^{31}\text{P}\{^1\text{H}\}$ NMR spectrum, tentatively assigned as [CpFe(P^{Ph}₂N^{Bn})₂(DBU)]BAR^F₄ (1-DBU). Subsequent treatment of H₂ did not form [1-H₂]⁺ or 1-H.

CpFe(P^{Ph}₂N^{Ph})₂Cl, (2-Cl). The complex was synthesized in a manner similar to 1-Cl, using [CpFe(CO)₂Cl] (0.467 g, 2.20 mmol) and P^{Ph}₂N^{Ph}₂ (1.000 g, 2.20 mmol). Recrystallization of the crude product in 20 mL of PhF layered with 200 mL of hexane yielded 1.070 g (81%) of black crystals suitable for X-ray diffraction. Anal. calcd. for C₃₃H₃₃N₂FeP₂Cl: C, 64.88; H, 5.45; N, 4.59. Found: C, 64.67; H, 5.46; N, 4.55. ¹H NMR (toluene-*d*₈): δ 8.15 (m, 3 H, C₆H₅), 7.27 (m, 4 H, C₆H₅), 7.21 (m, 2 H, C₆H₅), 7.08 (m, 2 H, C₆H₅), 6.75 (m, 4 H, C₆H₅), 6.57 (m, 2 H, C₆H₅), 4.08 (s, 5 H, C₅H₅), 4 (tt, 4 H, $J_{\text{HH}} = 12$ Hz, $J_{\text{PH}} = 3$ Hz, NCH_2P), 3.57 (d, $J_{\text{HH}} = 13$ Hz, 2 H, NCH_2P), 3.18 (dt, $J_{\text{HH}} = 12.5$ Hz, $J_{\text{PH}} = 8$ Hz, 2 H, NCH_2P). $^{31}\text{P}\{^1\text{H}\}$ NMR (CD₂Cl₂): δ 61.1 (s).

[CpFe(P^{Ph}₂N^{Ph})₂(H₂)]BAR^F₄ ([2-H₂]⁺). [2-H₂]⁺ was prepared using the same procedure as described for [CpFe(P^{Ph}₂N^{Bn})₂(H₂)]BAR^F₄ ([1-H₂]⁺) (yield, 79% based on 0.200 mmol (0.122 g) [CpFe(P^{Ph}₂N^{Ph})₂-Cl], (2-Cl)). ¹H NMR (PhCl-d_3): δ 8.02 (s, 8 H, B(C₆F₆H₃)₄), 7.33 (s, 4 H, B(C₆F₆H₃)₄), 7.20 (m, 8 H, C₆H₅), 7.05 (t, 2 H, C₆H₅), 6.70 (m, 8 H, C₆H₅), 6.30 (d, 2 H, C₆H₅), 3.78 (s, 5 H, C₅H₅), 3.52 (d, $J_{\text{HH}} = 15$ Hz, 2H, NCH_2P), 3.36 (d, $J_{\text{HH}} = 15$ Hz, Hz NCH_2P), 3.08 (d, $J_{\text{HH}} = 15$ Hz, 2 H, NCH_2P), 2.59 (d, 2 H, $J_{\text{HH}} = 15$ Hz, NCH_2P), -12.68 (s, 2 H, FeH_2). $^{31}\text{P}\{^1\text{H}\}$ NMR (PhCl-d_3): δ 56.0 (s).

[CpFe(P^{Ph}₂N^{Ph})₂(HD)]BAR^F₄ ([2-HD]⁺). Complex [2-HD]⁺ was prepared from 2-Cl (0.012 g, 0.020 mmol) and HD gas (1.0 atm.) in a

J. Young NMR tube using 0.6 mL of PhCl-d_3 solvent according to the procedure used for [1-HD]⁺. ¹H NMR (PhCl-d_3) for [2-HD]⁺: δ -12.75 (t, $J_{\text{HD}} = 27.5$ Hz, 1 H, Fe(HD)).

CpFe(P^{Ph}₂N^{Ph})₂(H), (2-H). Complex 2-H was prepared by both methods described above for 1-H. Method A gave an isolated yield of 75% (0.173 g, based on 2-Cl, 0.243 g, 0.400 mmol). Single crystals suitable for X-ray diffraction study were grown from an ether solution stored at -35 °C. Anal. calcd. for C₃₅H₃₈N₂FeP₂: C, 69.54; H, 6.34; N, 4.63. Found: C, 69.26; H, 6.28; N, 4.63. ¹H NMR (THF-*d*₈): δ 7.88 (m, 4 H, C₆H₅), 7.47 (m, 6 H, C₆H₅), 7.15 (m, 4 H, C₆H₅), 6.96 (d, $J_{\text{HH}} = 25$ Hz, 2 H, C₆H₅), 6.87 (d, $J_{\text{HH}} = 25$ Hz, 2 H, C₆H₅), 6.72 (t, $J_{\text{HH}} = 10$ Hz, 1 H, C₆H₅), 6.61 (t, $J_{\text{HH}} = 10$ Hz, 2 H, C₆H₅), 4.31 (d, $J_{\text{HH}} = 20$ Hz, 2 H, NCH_2P), 3.90 (m, 4 H, NCH_2P), 3.82 (d, $J_{\text{HH}} = 20$ Hz, 2 H, NCH_2P), 3.72 (s, 5 H, C₅H₅), 2.90 (d, $J_{\text{HH}} = 20$ Hz, 2 H, NCH_2P), -15.74 (t, $J_{\text{PH}} = 50$ Hz, 1 H, FeH). ^{31}P NMR (THF-*d*₈): δ 73.3 (s).

Protonation of 1-H and 2-H. HBF₄·Et₂O (30 μL of a suspension prepared by adding 0.1 mL of HBF₄·Et₂O to PhF, then diluting to 1.00 mL) was added dropwise in a NMR tube containing a solution of 1-H (or 2-H) (0.06 g, 0.001 mmol, in 0.6 mL of PhCl-d_3) under H₂ (1.0 atm), until the reaction was complete, as indicated by ¹H NMR spectroscopy. The formation of the [1-H₂]⁺ and [2-H₂]⁺ was confirmed by ¹H and ³¹P NMR spectroscopy.

CpFe(P^{Ph}₂C₅)Cl, (3-Cl-a). The complex was synthesized according to the procedure for 1-Cl using [CpFe(CO)₂Cl] (0.467 g, 2.20 mmol) and P^{Ph}₂C₅ (0.8 g, 2.20 mmol). Two isomers were identified by ³¹P NMR spectroscopy in a ratio of about 1:0.15. The minor isomer was removed by washing with a solvent mixture (2:1 THF:hexane, 2 × 20 mL). The yield for the major isomer is 0.566 g (61%). Single crystals suitable for X-ray diffraction were grown from a CH₂Cl₂ solution layered with hexane. Anal. calcd. for C₂₂H₂₅N₂P₂FeCl: C, 59.69; H, 5.69. Found: C, 59.61; H, 5.46; N, 5.46. For the major isomer: ¹H NMR (CD₂Cl₂): δ 8.1 (m, 4 H, C₆H₅), 7.54 (m, 6 H, C₆H₅), 4.07 (s, 5 H, C₅H₅), 2.66 (m, 2 H, P(CH₂)₃P), 2.41 (m, 1 H, P(CH₂)₃P), 2.07 (m, 1 H, P(CH₂)₃P), 2.01 (m, 2 H, P(CH₂)₂P), 1.97 (m, 2 H, P(CH₂)₂P), 1.80 (m, 2 H, P(CH₂)₃P). ^{31}P NMR (CD₂Cl₂): δ 80.11 (s). For the minor isomer: ^{31}P NMR (CD₂Cl₂): δ 85.50 (s).

[CpFe(P^{Ph}₂C₅)(H₂)]₂, [3-H₂]⁺. Complex [3-H₂]⁺ was generated from 3-Cl (0.009 g, 0.020 mmol) and H₂ (1.0 atm.) using the same procedure as described for [CpFe(P^{Ph}₂N^{Bn})₂(H₂)]BAR^F₄ (1-H₂). Two isomers ([3-H₂-a]⁺ and [3-H₂-b]⁺) of [3-H₂]⁺ were identified by ¹H NMR and ³¹P NMR spectroscopy in a ratio of about 1:0.5. In the ¹H NMR spectrum, the two isomers are distinguished by the Cp ring proton resonances and the H₂ ligand resonance, while the signals of the aromatic protons (from δ 6.7 to 8.01) and methylene protons (from δ 6 to 1.89) appear as overlapping resonances. For the major isomer ([3-H₂-a]⁺), ¹H NMR (PhCl-d_3): δ 3.83 (s, 5 H, C₅H₅), -13.79 (s, 2 H, FeH_2). $^{31}\text{P}\{^1\text{H}\}$ NMR (PhCl-d_3): δ 83.70 (s). For the minor isomer ([3-H₂-b]⁺), ¹H NMR (PhCl-d_3): δ 3.57 (s, 5 H, C₅H₅), -13.04 (s, 2 H, FeH_2). $^{31}\text{P}\{^1\text{H}\}$ NMR (PhCl-d_3): δ 85.47 (s).

[CpFe(P^{Ph}₂C₅)(HD)]₂, [3-HD]⁺. Complex [3-HD]⁺ was prepared from 3-Cl (0.009 g, 0.020 mmol) and HD gas (1.0 atm.) in a J. Young NMR tube using 0.6 mL PhCl-d_3 solvent according to the procedure of [1-HD]⁺. The reaction was followed by ¹H NMR spectroscopy. For the major isomer ([3-HD-a]⁺), ¹H NMR (PhCl-d_3): δ -13.89 (tt, $J_{\text{HD}} = 25$ Hz, $J_{\text{PH}} = 8.3$ Hz, 1 H, Fe(HD)). For the minor isomer ([3-HD-b]⁺), ¹H NMR (PhCl-d_3): δ -13.13 (tt, $J_{\text{HD}} = 25$ Hz, $J_{\text{PH}} = 4.5$ Hz, 1 H, Fe(HD)). A $^1\text{H}\{^{31}\text{P}\}$ NMR spectrum was recorded to confirm the phosphorus and HD coupling. The triplet of triplets of the HD ligand resonance for each isomer observed in the ¹H NMR spectrum collapsed to a triplet.

Deprotonation of [CpFe(P^{Ph}₂C₅)(H₂)₂]⁺, ([3-H₂]⁺). To the solution of [3-H₂]⁺ (prepared in situ in a NMR tube) was added 4 μL of DBU (ca. 4 equiv). After 10 min shaking, both ¹H NMR and $^{31}\text{P}\{^1\text{H}\}$ NMR spectroscopic monitoring indicated two isomers (3-H-a and 3-H-b) of 3-H formed in a ratio of about 1:0.22. For the major isomer, [3-H-a]⁺, ¹H NMR (PhCl-d_3): δ -17.30 (t, $J_{\text{PH}} = 65$ Hz, 1 H, Fe(H)). $^{31}\text{P}\{^1\text{H}\}$ NMR (PhCl-d_3): δ 96.12 (s). For the minor isomer, [3-H-b]⁺, ¹H NMR (PhCl-d_3): δ -13.13 (t, $J_{\text{PH}} = 65$ Hz, 1 H, Fe(H)). $^{31}\text{P}\{^1\text{H}\}$ NMR (PhCl-d_3): δ 100.95 (s).

CpFe(P^{Ph}₂C₅)(H), (3-H-a). Complex 3-H-a was prepared from 3-Cl-a (0.133 g, 0.300 mmol) and LiAlH₄ (0.035 g, ca. 3 equiv) by following method A described above for 1-H. There was only a trace amount of the minor isomer (3-H-b) present, as indicated by ¹H NMR and ³¹P{¹H} NMR spectroscopy. The minor isomer was removed by washing with Et₂O (2 × 5 mL). The major isomer, 3-H-a, was isolated in a yield of 0.091 g (74%). Anal. calcd. for C₂₂H₂₆P₂Fe: C, 64.73; H, 6.42. Found: C, 64.94; H, 6.58. ¹H NMR (THF-*d*₆): δ 7.86 (s, 4 H, C₆H₅), 7.39 (m, 6 H, C₆H₅), 4.02 (s, 5 H, C₅H₅), 2.30 (m, 3 H, P(CH₂)₃P, P(CH₂)₂P), 1.96 (m, 5 H, P(CH₂)₃P, P(CH₂)₂P), 1.38 (m, 2 H, P(CH₂)₃P), -17.30 (t, *J*_{PH} = 28 Hz, 1 H, Fe(H)). ³¹P{¹H} NMR (CD₂Cl₂, ppm): δ 96.12 (s).

Protonation of 3-H-a. A solution of 3-H-a (0.008 g, 0.020 mmol, in 0.6 mL of PhCl-*d*₅) under H₂ (1.0 atm) in an NMR tube was cooled to -60 °C using a dry ice/CHCl₃ slush bath. One equiv HBF₄·Et₂O (30 μL of a suspension prepared by adding 0.1 mL of HBF₄·Et₂O to PhF, then diluting to 1.00 mL) was added. The NMR tube was placed in a NMR spectrometer precooled to -40 °C. A series of spectra (¹H NMR and ³¹P{¹H} NMR) were recorded at -35, -25, -15, 0, 15, and 25 °C. Only [3-H₂-a]⁺ was observed at -35 and -25 °C. The second isomer, [3-H₂-b]⁺ started to appear at -15 °C.

H₂/D₂ Scrambling of [1-H₂]⁺ and [2-H₂]⁺. A NMR tube was loaded with 0.029 g (0.020 mmol) of 1-H₂ (or 2-H₂) under H₂ (1.0 atm) in 0.6 mL of PhCl-*d*₅. After the first ¹H NMR spectrum was recorded, the NMR tube was injected with D₂ (1.0 atm, 3 mL) to fill the headspace. D₂ was mixed with the solution by shaking for 10 min. The H₂/D₂ scrambling was monitored by ¹H NMR over 12 h. The formation of [1-HD]⁺ (or [2-HD]⁺) and HD were established by observing a triplet at δ -12.71 (or -12.75 for [2-HD]⁺) and another triplet at δ 4.22, respectively. In the case of [1-H₂]⁺, a ²H NMR spectrum was recorded after 2 h. ²H NMR: δ -12.64 for [1-HD]⁺, -12.90 for [1-D₂]⁺.

H₂/D₂ Exchange of [3-H₂]⁺ without External Base. Complex [3-H₂]⁺ (0.027 g, 0.020 mmol) under H₂ (1.0 atm.) in 0.6 mL of PhCl-*d*₅ was prepared in an NMR tube. After the first ¹H NMR spectrum was recorded, the NMR tube was injected with D₂ (1.0 atm, 3 mL) to fill the headspace. D₂ was mixed with the solution by shaking for 10 min. The ¹H NMR and ³¹P{¹H} spectra were monitored by NMR spectroscopy over 19 h. No H₂/D₂ scrambling occurred; [3-D₂]⁺ instead of [3-HD]⁺ was identified by ³¹P{¹H} NMR spectroscopy over time and a ²H NMR spectrum recorded at 15 h. ³¹P{¹H} NMR (PhCl-*d*₅) for [3-H₂]⁺: δ 85.47 (s) (minor isomer), 83.70 (s) (major isomer); ³¹P{¹H} NMR (PhCl-*d*₅) for [3-D₂]⁺: δ 85.40 (s) (minor isomer), 83.58 (s) (major isomer). ²H NMR for [3-D₂]⁺: δ -13.32 (minor isomer, s, 2 D, Fe-D₂), -14.08 (major isomer, s, 2 D, Fe-D₂).

H₂/D₂ Scrambling of [3-H₂]⁺ in the Presence of an External Base (Aniline or Benzylamine). Complex [3-H₂]⁺ (0.027 g, 0.020 mmol) under H₂ (1.0 atm.) in 0.6 mL of PhCl-*d*₅ was prepared in an NMR tube. After the first ¹H NMR spectrum was recorded, the NMR tube was injected with D₂ (1.0 atm, 3 mL) to fill its headspace, and subsequently, 2 equiv aniline (0.040 mmol, 40 μL, 1.0 M in PhF) or benzylamine (0.040 mmol, 44 μL, 0.92 M in PhF) was added. The mixture was shaken for 10 min, then H₂/D₂ scrambling was monitored by ¹H NMR spectroscopy over 15 h. Two triplets attributed to the two isomers of Fe(HD) gradually grew in; HD was characterized as the triplet at δ 4.33. ³¹P NMR spectra were recorded before adding D₂, at 10 min and at 15 h after adding D₂, respectively. In the case of aniline, a ²H NMR spectrum was recorded after 15 h. ²H NMR for [3-HD]⁺: δ -13.00 (minor isomer, s, 1 D, Fe-HD), -13.77 (major isomer, s, 1 D, Fe-HD). ²H NMR for [3-D₂]⁺: δ -13.32 (minor isomer, s, 2 D, Fe-D₂), -14.08 (major isomer, s, 2 D, Fe-D₂).

H/D Exchange of Fe-H (1-H, 2-H, and 3-H) with D₂O. In a representative experiment, 0.01 mmol of 1-H (2-H or 3-H) was dissolved in 0.6 mL of THF-*d*₈ in a NMR tube under argon. Initial ¹H NMR and ³¹P NMR spectra were recorded. Ten μL D₂O (ca. 56 equiv) was added to the sample. The disappearance of hydride signal was followed by ¹H NMR spectroscopy by comparing relative integrals of hydride and Cp resonances. Only trace hydride was detected after 4 min, which is the time required for manipulation. Due to the fast kinetics, the rate was not determined. The half-life time is estimated to

be about 2 min. The formation of the Fe-D species was confirmed by ³¹P NMR and ²H NMR. ²H NMR for 1-D, -16.03 (t, *J*_{PD} = 10 Hz, 1 D, Fe(D)); ²H NMR for 2-D, -15.71 (t, *J*_{PD} = 10 Hz, 1 D, Fe(D)); ²H NMR for 3-D, -17.30 (t, *J*_{PD} = 10 Hz, 1 D, Fe(D)).

Attempted Electrochemical H₂ Oxidation Catalyzed by 1-H.

An 1 mL of PhF solution containing 1.0 mM of 1-H was maintained under atm argon. The first CV trace was recorded for 1-H at 100 mV/s. Five equiv of base (DBU) were added, and cyclic voltammograms were recorded. Then the atmosphere was replaced by 1.0 atm H₂, and the third CV was recorded. No apparent catalytic current was observed under H₂ (see Figure 7). Similar results were obtained in the experiment in which DBU was added in the presence of H₂.

Attempted Chemical Oxidation of D₂ Catalyzed by 1-H.

1-H (0.006 g, 0.010 mmol) and 5 equiv of the oxidant, [Cp₂Fe]PF₆ (0.016 mg, 0.050 mmol) were loaded into a NMR tube under 1.0 atm D₂. Then 1.0 mL of PhF solution containing DBU (0.050 mmol) was injected into NMR tube. The reaction solution was monitored by ²H NMR spectroscopy for several hours but provided no indication of the formation of [DBU-D⁺].

■ ASSOCIATED CONTENT

Supporting Information

NMR data for 1-Cl, [1-CO]Cl, [1-H₂]BAR₄^F, [2-H₂]BAR₄^F, [2-(HD)]BAR₄^F, 2-H, 3-Cl, [3-H₂]BAR₄^F, and [3-H₂]BAR₄^F; IR spectrum of [1-CO]Cl, ESI-MS data of 1⁺-BAR₄^F; electrochemical data for 1-Cl, [1-H₂]BAR₄^F, 1⁺-BAR₄^F, 1-H, 2-Cl, 2-H, 3-Cl-a, and 3-H-a; X-ray structures and selected distances and angles of 2-Cl and 2-H; structural comparison of the X-ray structure and the DFT calculated structure of [1-H₂]⁺ and 1-H; DFT calculation on the intermolecular H₂ cleavage by [1-H₂]⁺; crystallographic data and .cif files for 1-Cl, [1-CO]Cl, [1-H₂]BAR₄^F, 1-H, 2-Cl, 2-H, and 3-Cl-a; and complete ref 32. This material is available free of charge via the Internet at <http://pubs.acs.org>.

■ AUTHOR INFORMATION

Corresponding Author

*daniel.dubois@pnnl.gov; morris.bullock@pnnl.gov

Notes

The authors declare no competing financial interest.

■ ACKNOWLEDGMENTS

We thank the U.S. Department of Energy, Office of Basic Energy Sciences, Division of Chemical Sciences, Geosciences and Biosciences, for support of this research. S.C. (DFT computations) and M.J.O. (NMR experiments) were supported by the Center for Molecular Electrocatalysis, an Energy Frontier Research Center funded by the U.S. Department of Energy, Office of Science, Office of Basic Energy Sciences. Pacific Northwest National Laboratory is operated by Battelle for the U.S. Department of Energy.

■ REFERENCES

- (1) (a) Frey, M. *ChemBioChem* **2002**, *3*, 153–160. (b) Tard, C.; Pickett, C. J. *Chem. Rev.* **2009**, *109*, 2245–2274. (c) Peters, J. W.; Lanzilotta, W. N.; Lemon, B. J.; Seefeldt, L. C. *Science* **1998**, *282*, 1853–1858.
- (2) (a) Fontecilla-Camps, J. C.; Volbeda, A.; Cavazza, C.; Nicolet, Y. *Chem. Rev.* **2007**, *107*, 4273–4303.
- (3) (a) Connolly, P.; Espenson, J. H. *Inorg. Chem.* **1986**, *25*, 2684–2688. (b) Hu, X.; Brunschwig, B. S.; Peters, J. C. *J. Am. Chem. Soc.* **2007**, *129*, 8988–8998. (c) Liu, T.; Darensbourg, M. Y. *J. Am. Chem. Soc.* **2007**, *129*, 7008–7009. (d) Darensbourg, M. Y.; Lyon, E. J.; Zhao, X.; Georgakaki, I. P. *Proc. Natl. Acad. Sci. U.S.A.* **2003**, *100*, 3683–3688. (e) Felton, G. A. N.; Vannucci, A. K.; Chen, J.; Lockett, L. T.;

- Okumura, N.; Petro, B. J.; Zakai, U. I.; Evans, D. H.; Glass, R. S.; Lichtenberger, D. L. *J. Am. Chem. Soc.* **2007**, *129*, 12521–12530.
- (f) Gloaguen, F.; Rauchfuss, T. B. *Chem. Soc. Rev.* **2009**, *38*, 100–108.
- (g) Barton, B. E.; Rauchfuss, T. B. *J. Am. Chem. Soc.* **2010**, *132*, 14877–14885.
- (h) Olsen, M. T.; Bruschi, M.; De Gioia, L.; Rauchfuss, T. B.; Wilson, S. R. *J. Am. Chem. Soc.* **2008**, *130*, 12021–12030.
- (i) Artero, V.; Fontecave, M. *Coord. Chem. Rev.* **2005**, *249*, 1518–1535.
- (j) Baffert, C.; Artero, V.; Fontecave, M. *Inorg. Chem.* **2007**, *46*, 1817–1824.
- (k) Appel, A. M.; DuBois, D. L.; Rakowski DuBois, M. *J. Am. Chem. Soc.* **2005**, *127*, 12717–12726.
- (l) Sun, Y.; Bigi, J. P.; Piro, N. A.; Tang, M. L.; Long, J. R.; Chang, C. J. *J. Am. Chem. Soc.* **2011**, *133*, 9212–9215.
- (m) Karunadasa, H. I.; Chang, C. J.; Long, J. R. *Nature* **2010**, *464*, 1329–1333.
- (n) Lee, C. H.; Dogutan, D. K.; Nocera, D. G. *J. Am. Chem. Soc.* **2011**, *133*, 8775–8777.
- (o) McNamara, W. R.; Han, Z.; Alperin, P. J.; Brennessel, W. W.; Holland, P. L.; Eisenberg, R. *J. Am. Chem. Soc.* **2011**, *133*, 15368–15371.
- (4) (a) Rakowski DuBois, M.; DuBois, D. L. *C. R. Chimie* **2008**, *11*, 805–817. (b) Rakowski DuBois, M.; DuBois, D. L. *Chem. Soc. Rev.* **2009**, *38*, 62–72. (c) Rakowski Dubois, M.; Dubois, D. L. *Acc. Chem. Res.* **2009**, *42*, 1974–1982. (d) Wilson, A. D.; Shoemaker, R. K.; Miedaner, A.; Muckerman, J. T.; DuBois, D. L.; Rakowski DuBois, M. *Proc. Natl. Acad. Sci. U.S.A.* **2007**, *104*, 6951–6956. (e) Helm, M. L.; Stewart, M. P.; Bullock, R. M.; Rakowski DuBois, M.; DuBois, D. L. *Science* **2011**, *333*, 863–866. (f) Yang, J. Y.; Bullock, R. M.; Shaw, W. J.; Twamley, B.; Frazee, K.; Rakowski DuBois, M.; DuBois, D. L. *J. Am. Chem. Soc.* **2009**, *131*, 5935–5945. (g) Yang, J. Y.; Chen, S.; Dougherty, W. G.; Kassel, W. S.; Bullock, R. M.; DuBois, D. L.; Raugai, S.; Rousseau, R.; Dupuis, M.; Rakowski DuBois, M. *Chem. Commun.* **2010**, *46*, 8618–8620. (h) Kilgore, U.; Roberts, J.; Pool, D. H.; Appel, A.; Stewart, M.; Rakowski DuBois, M.; Dougherty, W. G.; Kassel, W. S.; Bullock, R. M.; DuBois, D. L. *J. Am. Chem. Soc.* **2011**, *133*, 5861–5872. (i) Curtis, C. J.; Miedaner, A.; Ciancanelli, R.; Ellis, W. W.; Noll, B. C.; Rakowski DuBois, M.; DuBois, D. L. *Inorg. Chem.* **2003**, *42*, 216–227. (j) Kilgore, U. J.; Stewart, M. P.; Helm, M. L.; Dougherty, W. G.; Kassel, W. S.; Rakowski DuBois, M.; DuBois, D. L.; Bullock, R. M. *Inorg. Chem.* **2011**, *50*, 10908–10918.
- (5) Wilson, A. D.; Newell, R. H.; McNevin, M. J.; Muckerman, J. T.; Rakowski DuBois, M.; DuBois, D. L. *J. Am. Chem. Soc.* **2006**, *128*, 358–366.
- (6) (a) Jacobsen, G. M.; Yang, J. Y.; Twamley, B.; Wilson, A. D.; Bullock, R. M.; Rakowski DuBois, M.; DuBois, D. L. *Energy Environ. Sci.* **2008**, *1*, 167–174. (b) Wiedner, E. S.; Yang, J. Y.; Dougherty, W. G.; Kassel, W. S.; Bullock, R. M.; Rakowski DuBois, M.; DuBois, D. L. *Organometallics* **2010**, *29*, 5390–5401.
- (7) Fan, H. J.; Hall, M. B. *J. Am. Chem. Soc.* **2001**, *123*, 3828–3829.
- (8) *Catalysis without Precious Metals*; Bullock, R. M., Ed.; Wiley-VCH: Weinheim, Germany, 2010.
- (9) Henry, R. M.; Shoemaker, R. K.; DuBois, D. L.; Rakowski DuBois, M. *J. Am. Chem. Soc.* **2006**, *128*, 3002–3010.
- (10) (a) Jacobsen, G. M.; Shoemaker, R. K.; McNevin, M. J.; Rakowski DuBois, M.; DuBois, D. L. *Organometallics* **2007**, *26*, 5003–5009. (b) Jacobsen, G. M.; Shoemaker, R. K.; Rakowski DuBois, M.; DuBois, D. L. *Organometallics* **2007**, *26*, 4964–4971.
- (11) (a) Barton, B. E.; Olsen, M. T.; Rauchfuss, T. B. *J. Am. Chem. Soc.* **2008**, *130*, 16834–16835. (b) Barton, B. E.; Rauchfuss, T. B. *Inorg. Chem.* **2008**, *47*, 2261–2263.
- (12) (a) Ott, S.; Kritikos, M.; Åkermark, B.; Sun, L.; Lomoth, R. *Angew. Chem., Int. Ed.* **2004**, *43*, 1006–1009. (b) Schwartz, L.; Eilers, G.; Eriksson, L.; Gogoll, A.; Lomoth, R.; Ott, S. *Chem. Commun.* **2006**, 520–522. (c) Gao, W. M.; Liu, J. H.; Åkermark, B.; Sun, L. C. *Inorg. Chem.* **2006**, *45*, 9169–9171. (d) Song, L. C.; Wang, H. T.; Ge, J. H.; Mei, S. Z.; Gao, J.; Wang, L. X.; Gai, B.; Zhao, L. Q.; Yan, J.; Wang, Y. Z. *Organometallics* **2008**, *27*, 1409–1416. (e) Ezzaher, S.; Capon, J. F.; Gloaguen, F.; Petillon, F. Y.; Schollhammer, P.; Talarmin, J.; Kervarec, N. *Inorg. Chem.* **2009**, *48*, 2–4. (f) Chiang, M.-H.; Liu, Y.-C.; Yang, S.-T.; Lee, G.-H. *Inorg. Chem.* **2009**, *48*, 7604–7612.
- (13) Roger, C.; Hamon, P.; Toupet, L.; Rabaa, H.; Saillard, J. Y.; Hamon, J. R.; Lapinte, C. *Organometallics* **1991**, *10*, 1045–1054.
- (14) (a) Douglas, B. M., D.; Alexander, J. *Concepts and Models of Inorganic Chemistry*; Wiley & Sons: New York, 1994, p 102. (b) Drago, R. S. *Physical Methods for Chemists*; Saunders: New York, 1992; p 99.
- (15) Chinn, M. S.; Heinekey, D. M. *J. Am. Chem. Soc.* **1990**, *112*, 5166–5175.
- (16) Jia, G.; Ng, W. S.; Yao, J.; Lau, C.-P.; Chen, Y. *Organometallics* **1996**, *15*, 5039–5045.
- (17) Luther, T. A.; Heinekey, D. M. *Inorg. Chem.* **1998**, *37*, 127–132.
- (18) Maltby, P. A.; Schlaf, M.; Steinbeck, M.; Lough, A. J.; Morris, R. H.; Klooster, W. T.; Koetzle, T. F.; Srivastava, R. C. *J. Am. Chem. Soc.* **1996**, *118*, 5396–5407.
- (19) Morris, R. H. *Coord. Chem. Rev.* **2008**, *252*, 2381–2394.
- (20) Kaljurand, I.; Kutt, A.; Soovali, L.; Rodima, T.; Maemets, V.; Leito, I.; Koppel, I. A. *J. Org. Chem.* **2005**, *70*, 1019–1028.
- (21) Cotrait, M.; Bideau, J. P.; Gallois, B.; Ruiz, J.; Astruc, D. *Bull. Soc. Chim. Fr.* **1992**, *129*, 329–334.
- (22) Bau, R.; Teller, R. G.; Kirtley, S. W.; Koetzle, T. F. *Acc. Chem. Res.* **1979**, *12*, 176–183.
- (23) Toto, S. D.; Arbuckle, B. W.; Bharadwaj, P. K.; Doi, J. T.; Musker, W. K. *Phosphorus, Sulfur Silicon Relat. Elem.* **1991**, *56*, 27–38.
- (24) Brooks, P. J.; Gallagher, M. J.; Sarroff, A.; Bowyer, M. *Phosphorus, Sulfur Silicon Relat. Elem.* **1989**, *44*, 235–247.
- (25) Gusev, D. G.; Kuhlman, R. L.; Renkema, K. B.; Eisenstein, O.; Caulton, K. G. *Inorg. Chem.* **1996**, *35*, 6775–6783.
- (26) (a) Hamon, P.; Toupet, L.; Hamon, J.-R.; Lapinte, C. *Organometallics* **1996**, *15*, 10–12. (b) Argouarch, G.; Hamon, P.; Toupet, L.; Hamon, J.-R.; Lapinte, C. *Organometallics* **2002**, *21*, 1341–1348.
- (27) Leal, A. d. I. J.; Tenorio, M. J.; Puerta, M. C.; Valerga, P. *Organometallics* **1995**, *14*, 3839–3847.
- (28) (a) Becke, A. D. *J. Chem. Phys.* **1993**, *98*, 5648–5652. (b) Perdew, J. P. *Phys. Rev. B* **1986**, *33*, 8822–8824.
- (29) Andrae, D.; Häußermann, U.; Dolg, M.; Stoll, H.; Preuß, H. *Theor. Chem. Acc.* **1990**, *77*, 123–141.
- (30) Rassolov, V. A.; Pople, J. A.; Ratner, M. A.; Windus, T. L. *J. Chem. Phys.* **1998**, *109*, 1223–1229.
- (31) (a) Barone, V.; Cossi, M. *J. Phys. Chem. A* **1998**, *102*, 1995. (b) Cossi, M.; Rega, N.; Scalmani, G.; Barone, V. *J. Comput. Chem.* **2003**, *24*, 669–681.
- (32) Frisch, M. J. et al. *Gaussian 09*, revision B.01; Gaussian, Inc.: Wallingford, CT, 2009.
- (33) Bondi, A. J. *Phys. Chem.* **1964**, *68*, 441–451.
- (34) O'Hagan, M.; Shaw, W. J.; Raugai, S.; Chen, S.; Yang, J. Y.; Kilgore, U. J.; DuBois, D. L.; Bullock, R. M. *J. Am. Chem. Soc.* **2011**, *133*, 14301–14312.
- (35) (a) Custelcean, R.; Jackson, J. E. *Chem. Rev.* **2001**, *101*, 1963–1980. (b) Stevens, R. C.; Bau, R.; Milstein, D.; Blum, O.; Koetzle, T. F. *J. Chem. Soc., Dalton Trans.* **1990**, 1429–1432. (c) Lee, J. C.; Rheingold, A. L.; Muller, B.; Pregosin, P. S.; Crabtree, R. H. *J. Chem. Soc., Chem. Commun.* **1994**, 1021–1022. (d) Peris, E.; Lee, J. C.; Rambo, J. R.; Eisenstein, O.; Crabtree, R. H. *J. Am. Chem. Soc.* **1995**, *117*, 3485–3491. (e) Lough, A. J.; Park, S.; Ramachandran, R.; Morris, R. H. *J. Am. Chem. Soc.* **1994**, *116*, 8356–8357. (f) Siegbahn, P. E. M.; Eisenstein, O.; Rheingold, A. L.; Koetzle, T. F. *Acc. Chem. Res.* **1996**, *29*, 348–354.
- (36) Bard, A. J.; Faulkner, L. R. *Electrochemical Methods: Fundamentals and Applications*; 2nd ed.; John Wiley & Sons: New York, 2001.
- (37) Tilset, M.; Fjeldahl, I.; Hamon, J.-R.; Hamon, P.; Toupet, L.; Saillard, J.-Y.; Costuas, K.; Haynes, A. *J. Am. Chem. Soc.* **2001**, *123*, 9984–10000.
- (38) Lever, A. B. P. *Inorg. Chem.* **1990**, *29*, 1271–1285.
- (39) Morris, R. H. *Inorg. Chem.* **1992**, *31*, 1471–1478.
- (40) (a) Hoberg, H.; Peres, Y.; Kruger, C.; Tsay, Y. H. *Angew. Chem., Int. Ed.* **1987**, *26*, 771–773. (b) Carver, C. T.; Benitez, D.; Miller, K. L.; Williams, B. N.; Tkatchouk, E.; Goddard, W. A.; Diaconescu, P. L. *J. Am. Chem. Soc.* **2009**, *131*, 10269–10278. (c) Williams, B. N.; Benitez, D.; Miller, K. L.; Tkatchouk, E.; Goddard, W. A.; Diaconescu, P. L. *J. Am. Chem. Soc.* **2011**, *133*, 4680–4683.

- (41) Welch, K. D.; Dougherty, W. G.; Kassel, W. S.; DuBois, D. L.; Bullock, R. M. *Organometallics* **2010**, *29*, 4532–4540.
- (42) Wilson, A. D.; Frazee, K.; Twamley, B.; Miller, S. M.; DuBois, D. L.; Rakowski DuBois, M. *J. Am. Chem. Soc.* **2008**, *130*, 1061–1068.
- (43) Angelici, R. J. *Acc. Chem. Res.* **1972**, *5*, 335–341.
- (44) Bautista, M. T.; Cappellani, E. P.; Drouin, S. D.; Morris, R. H.; Schweitzer, C. T.; Sella, A.; Zubkowski, J. *J. Am. Chem. Soc.* **1991**, *113*, 4876–4887.
- (45) Gilbertson, J. D.; Szymczak, N. K.; Tyler, D. R. *Inorg. Chem.* **2004**, *43*, 3341–3343.
- (46) (a) Hamon, J.-R.; Hamon, P.; Toupet, L.; Costuas, K.; Saillard, J.-Y. C. R. *Chimie* **2002**, *5*, 89–98. (b) Belkova, N. V.; Revin, P. O.; Epstein, L. M.; Vorontsov, E. V.; Bakhmutov, V. I.; Shubina, E. S.; Collange, E.; Poli, R. *J. Am. Chem. Soc.* **2003**, *125*, 11106–11115.
- (47) (a) Peters, J. W. *Curr. Opin. Struct. Biol.* **1999**, *9*, 670–676. (b) Adams, M. W. W. *Biochim. Biophys. Acta* **1990**, *1020*, 115–145.
- (48) Zhao, X.; Georgakaki, I. P.; Miller, M. L.; Mejia-Rodriguez, R.; Chiang, C. Y.; Darensbourg, M. Y. *Inorg. Chem.* **2002**, *41*, 3917–3928.
- (49) Abdur-Rashid, K.; Fong, T. P.; Greaves, B.; Gusev, D. G.; Hinman, J. G.; Landau, S. E.; Lough, A. J.; Morris, R. H. *J. Am. Chem. Soc.* **2000**, *122*, 9155–9171.
- (50) SAINT V6.63 Program for Reduction of Area Detector Data; Bruker AXS Inc.: Madison, WI, 1996.
- (51) Sheldrick, G. SADABS Program for Absorption Correction of Area Detector Frames; Bruker AXS Inc.: Madison, WI, 2007.
- (52) Sheldrick, G. SHELXS-97 Program for Crystal Structure Solution; Institut für Anorganische Chemie der Universität Göttingen: Göttingen, Germany, 1997.
- (53) Sheldrick, G. SHELXL-97 Program for Crystal Structure Refinement; Institut für Anorganische Chemie der Universität Göttingen: Göttingen, Germany, 1997.
- (54) Farrugia, L. *J. Appl. Crystallogr.* **1997**, *30*, 565.
- (55) Piper, T. S.; Cotton, F. A.; Wilkinson, G. J. *Inorg. Nucl. Chem.* **1955**, *1*, 165–174.
- (56) Frazee, K.; Wilson, A. D.; Appel, A. M.; Rakowski DuBois, M.; DuBois, D. L. *Organometallics* **2007**, *26*, 3918–3924.